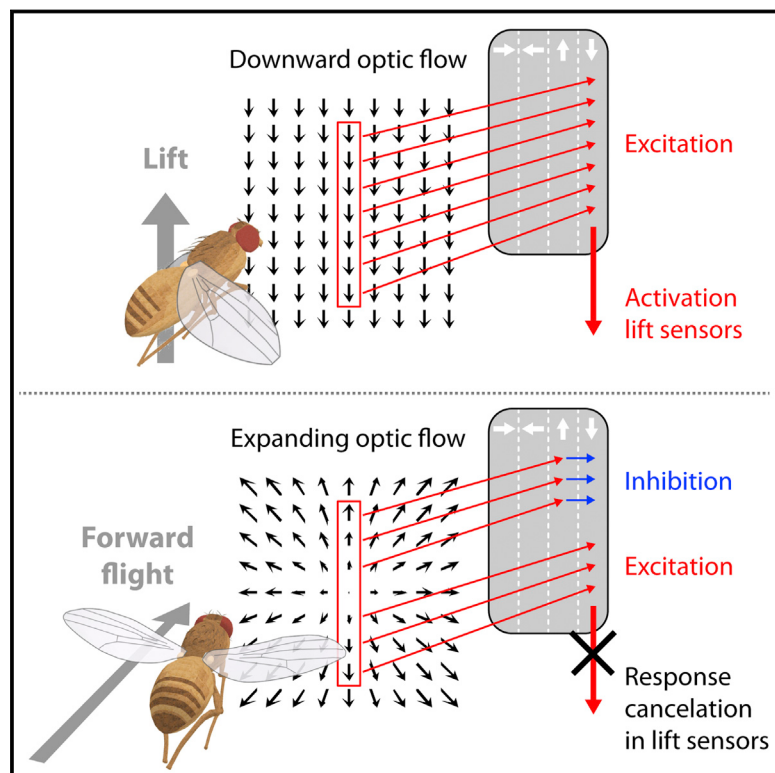


# Neural Circuit to Integrate Opposing Motions in the Visual Field

## Graphical Abstract



## Authors

Alex S. Mauss, Katarina Pankova,  
Alexander Arenz, Aljoscha Nern, Gerald  
M. Rubin, Alexander Borst

## Correspondence

amauss@neuro.mpg.de

## In Brief

Newly identified inhibitory neurons are central to an integrative circuit that enables *Drosophila* to process visual cues with opposite motions generated during flight. The neurons are required to discriminate between distinct complex motion patterns, indicating that neural processing of opposing cues can yield outcomes beyond the simple sum of two inputs.

## Highlights

- Discovery of bi-stratified glutamatergic lobula plate-intrinsic (LPI) interneurons
- LPI neurons provide visual null direction inhibition to wide-field tangential cells
- Blocking LPI activity leads to target neurons responding to inadequate motion cues
- Motion opponency thus increases flow-field selectivity

# Neural Circuit to Integrate Opposing Motions in the Visual Field

Alex S. Mauss,<sup>1,\*</sup> Katarina Pankova,<sup>1</sup> Alexander Arenz,<sup>1</sup> Aljoscha Nern,<sup>2</sup> Gerald M. Rubin,<sup>2</sup> and Alexander Borst<sup>1</sup>

<sup>1</sup>Max-Planck-Institute of Neurobiology, 82152 Martinsried, Germany

<sup>2</sup>Janelia Research Campus, Howard Hughes Medical Institute, Ashburn, VA 20147, USA

\*Correspondence: [amauss@neuro.mpg.de](mailto:amauss@neuro.mpg.de)

<http://dx.doi.org/10.1016/j.cell.2015.06.035>

## SUMMARY

When navigating in their environment, animals use visual motion cues as feedback signals that are elicited by their own motion. Such signals are provided by wide-field neurons sampling motion directions at multiple image points as the animal maneuvers. Each one of these neurons responds selectively to a specific optic flow-field representing the spatial distribution of motion vectors on the retina. Here, we describe the discovery of a group of local, inhibitory interneurons in the fruit fly *Drosophila* key for filtering these cues. Using anatomy, molecular characterization, activity manipulation, and physiological recordings, we demonstrate that these interneurons convey direction-selective inhibition to wide-field neurons with opposite preferred direction and provide evidence for how their connectivity enables the computation required for integrating opposing motions. Our results indicate that, rather than sharpening directional selectivity per se, these circuit elements reduce noise by eliminating non-specific responses to complex visual information.

## INTRODUCTION

Diverse sensory experiences can result in largely overlapping patterns of activation within sensory circuits yet require fundamentally different behavioral responses. An underlying key operation is the extraction of features relevant for specific behaviors by hierarchical layers of neuronal networks with increasing selectivity. A well-studied example of such feature extraction is the computation of the optic flow associated with self-motion—that is, the feedback motion cues created by an animal progressing through its environment. Across many animals studied, motion-sensitive neurons covering large receptive fields (those that receive input from cues spanning the visual field) tend to be motion opponent, i.e., are excited by motion along one and inhibited along the opposite direction (Collett and Blest, 1966; Duffy and Wurtz, 1991; Hausen, 1984; Ibbotson, 1991; Krapp and Hengstenberg, 1996; Wylie et al., 1998). However, the functional significance of motion opponency is unclear and has to date not been experimentally challenged. Here, we address this problem in *Drosophila*, which has emerged as a

powerful model system to study the mechanisms underlying motion vision (Borst et al., 2010).

The *Drosophila* optic lobe consists of four neuropiles called lamina, medulla, lobula, and lobula plate. Each of these neuropiles is built from about 750 repetitive columns arranged in a retinotopic way. Monopolar L1 and L2 cells, among others, receive photoreceptor input in the lamina and feed into two motion pathways (Bausenwein et al., 1992; Bausenwein and Fischbach, 1992; Clark et al., 2011; Joesch et al., 2010; Rister et al., 2007; Shinomiya et al., 2014; Silies et al., 2013; Takemura et al., 2013; Tuthill et al., 2013). Within each pathway, the direction of motion is computed separately, with the L1-pathway selectively processing motion of brightness increments (ON) and the L2-pathway motion of brightness decrements (OFF) (Eichner et al., 2011; Joesch et al., 2010, 2013). The outputs of the ON and OFF pathways are represented by arrays of small-field T4 and T5 cells, respectively. Each T4 and T5 cell is tuned to one of four cardinal directions and terminates in one of the four layers of the lobula plate such that opposite directions are represented in adjacent layers (Maisak et al., 2013) (layer 1: front to back; layer 2: back to front; layer 3: upward; layer 4: downward). These directions match the preferred directions of wide-field motion-sensitive tangential cells that extend their dendrites in the respective layers: horizontal system cells with dendrites in layer 1 depolarize during front-to-back motion and hyperpolarize during back-to-front motion, Hx cells in layer 2 exhibit the opposite tuning, and vertical system (VS) cells with dendrites mostly in layer 4 depolarize primarily during downward and hyperpolarize during upward motion (Hausen et al., 1980; Hopp et al., 2014; Schnell et al., 2010; Scott et al., 2002; Wasserman et al., 2015). With T4/T5 cells blocked, tangential cells lose all of their motion sensitivity (Schnell et al., 2012), and flies become completely motion blind (Bahl et al., 2013). Combining optogenetic stimulation of T4/T5 cells with various pharmacological antagonists, the connections between T4/T5 and tangential cells have recently been characterized as monosynaptic, excitatory, and cholinergic (Mauss et al., 2014). T4/T5 cells thus account for the depolarization of the tangential cells during preferred direction motion. What remains unclear is the mechanism and functional role of subtracting information about motion in the opposite or null direction.

Here, we characterize a hitherto unknown class of vertical system lobula plate intrinsic (LPI) neurons and demonstrate how they contribute to motion opponency. First, our anatomical and molecular characterization, as well as combined optogenetic stimulation and electrophysiological recordings, reveal that LPI

neurons are bi-stratified and inhibit tangential cells in single lobula plate layers via glutamatergic synapses. Second, we demonstrate by two-photon calcium imaging that LPi neurons are activated in response to motion directions similar to their presumed T4/T5 inputs and opposite to their postsynaptic targets. Third, genetically silencing LPi cell output selectively abolishes null direction inhibitory potential changes in tangential cells. We therefore conclude that LPi neurons hyperpolarize tangential cells during null direction motion through sign-inverting layer interactions, thus forming the cellular basis of motion opponency in the fly. As a final point, the identification of LPi neurons enabled us to experimentally address the long-sought functional relevance of motion opponency. As blocking the activity of LPi neurons renders their postsynaptic wide-field motion-sensitive neurons responsive to a variety of moving patterns, our experiments suggest that motion opponency is essential for flow-field selectivity, thereby improving the ability to reliably estimate self-motion trajectories based on complex visual information.

## RESULTS

### Anatomy of Lobula Plate Intrinsic Neurons

Previous work suggested the existence of yet unidentified lobula plate neurons underlying null direction responses in tangential cells (Mauss et al., 2014). Candidate neurons to fulfill this role are expected to possess a bi-stratified morphology covering either both horizontal (1 and 2) or both vertical (3 and 4) layers. To identify such cell types, we screened the Janelia *Drosophila* driver line collection (Jenett et al., 2012; Pfeiffer et al., 2008) and discovered two independent lines (R20D01, R38G02) containing neurons that exclusively innervate the two layers of the lobula plate vertical system. Moreover, putative presynaptic varicosities for each line are located in either layer 3 (R38G02) or 4 (R20D01), suggesting two distinct functional cell types. We confirmed the presynaptic nature of these varicosities by co-expressing GFP and the presynaptic reporter Synaptotagmin (Syt), which correspondingly localized to layer 3 (R38G02) and layer 4 (R20D01; Figures 1A–1B'). This anatomical layout indicates a complementary directed signal transfer from layer 3 to 4 in one and from layer 4 to 3 in the other cell type. Accordingly, these two new neuron types are termed LPi3-4 (lobula plate intrinsic) and LPi4-3, respectively. To reveal single-cell morphologies, we performed stochastic multicolor labeling of LPi cells (Figures 1C–1I) (Nern et al., 2015). Neurons in each line have vertically elongated arbors covering the lobula plate in partly segregated patches. While individual LPi neurons occupy lobula plate layers 3 and 4, their potential postsynaptic targets, the VS cells, have dendrites restricted to layer 4 only (Figures 1J and 1J').

### Transmitter Phenotype and Connectivity

We next investigated the transmitter phenotype of the LPi cells by immunostaining (LPi3-4 and LPi4-3) and mRNA profiling (Takemura et al., 2011) (LPi3-4). Both approaches revealed that LPi neurons express vesicular glutamate transporter (vGlut; Figures 2A–2C), while cholinergic and GABAergic markers could not be detected (Figures 2C and S1). Aptly, tangential cells express glutamate-gated chloride channel  $\alpha$  (GluCl $\alpha$ ; Figure 2C), in line with their hyperpolarizing responses to glutamate applica-

tion (Mauss et al., 2014). These results suggest that tangential cells receive inhibitory glutamatergic input from LPi neurons. To directly explore the synaptic connectivity between LPi neurons and tangential cells, we focused on LPi3-4 neurons, which provide putative synaptic input to the experimentally accessible VS cells in lobula plate layer 4 (Figure 1J). First, we labeled membrane contacts using the GRASP method (Feinberg et al., 2008) by expressing membrane-targeted CD4-spGFP1-10 and CD4-spGFP11 independently in LPi3-4 and VS cells using four different driver line combinations. In all cases, reconstituted fluorescence signal could be detected exclusively in lobula plate layer 4, indicating contact between LPi3-4 terminals and VS cell dendrites (Figures 2D and S2). To functionally determine the synaptic connectivity, we took an optogenetic approach previously used to establish connectivity between T4/T5 and tangential cells (Mauss et al., 2014): brief optogenetic stimulation of T4/T5 cells in blind, *norpA*<sup>7</sup> mutant flies evoked biphasic synaptic responses in VS cells with direct cholinergic excitation and delayed indirect inhibition (Figure 2E, red trace), the latter being sensitive to the GABA/glutamate receptor antagonist picrotoxin (Mauss et al., 2014). To test whether this inhibitory component could be conveyed by LPi3-4 cells, we optogenetically stimulated LPi3-4 cells expressing ChR2-H134R in blind flies while performing patch-clamp recordings from VS cells. VS cells responded to optogenetic LPi stimulation with picrotoxin-sensitive inhibitory potential changes (Figures 2E–2H) and onset latencies comparable to T4/T5-evoked excitation (Figure 2E). We conclude that LPi3-4 neurons provide fast inhibitory glutamatergic input to VS cells in layer 4 of the lobula plate.

### Visual Response Properties of LPi Neurons

Cholinergic T4/T5 cells represent the major motion-sensitive input to the lobula plate (Schnell et al., 2012), and their axons segregate into four layers according to their directional tuning (Maisak et al., 2013). LPi cells of a single type are thus expected to acquire direction selectivity by receiving excitatory input from T4/T5 cells in one of the two motion-opponent layers. To probe the LPi cells' visual response properties, we expressed the genetically encoded calcium indicator GCaMP5G (Akerboom et al., 2012) and recorded calcium signals (Denk et al., 1990; Maisak et al., 2013; Reiff et al., 2010) from putative presynaptic boutons in the lobula plate while stimulating flies with pattern motion (Figures 3A and 3B). Both LPi cell types responded in a strictly direction-selective way to moving square-wave gratings. Importantly, LPi3-4 cells were tuned to upward motion and LPi4-3 cells to the opposite, i.e., downward direction (Figures 3C and 3D). Thus, the preferred direction of LPi3-4 cells matches the one of T4/T5 cells terminating in layer 3, and the preferred direction of LPi4-3 cells corresponds to the one of T4/T5 cells terminating in layer 4. We next tested LPi responses to gratings moving with different velocities. A correlation type motion detector as implemented in flies results in a velocity tuning as a linear function of the spatial pattern wavelength. This feature is reflected in the T4/T5 and tangential cell responses, which exhibit an optimal temporal frequency of ~1 Hz in quiescent flies (Joesch et al., 2008; Maisak et al., 2013; Schnell et al., 2010). Likewise, LPi3-4 and LPi4-3 cells both had velocity tuning peaks at 24° s<sup>-1</sup> for gratings with a spatial wavelength of 24°

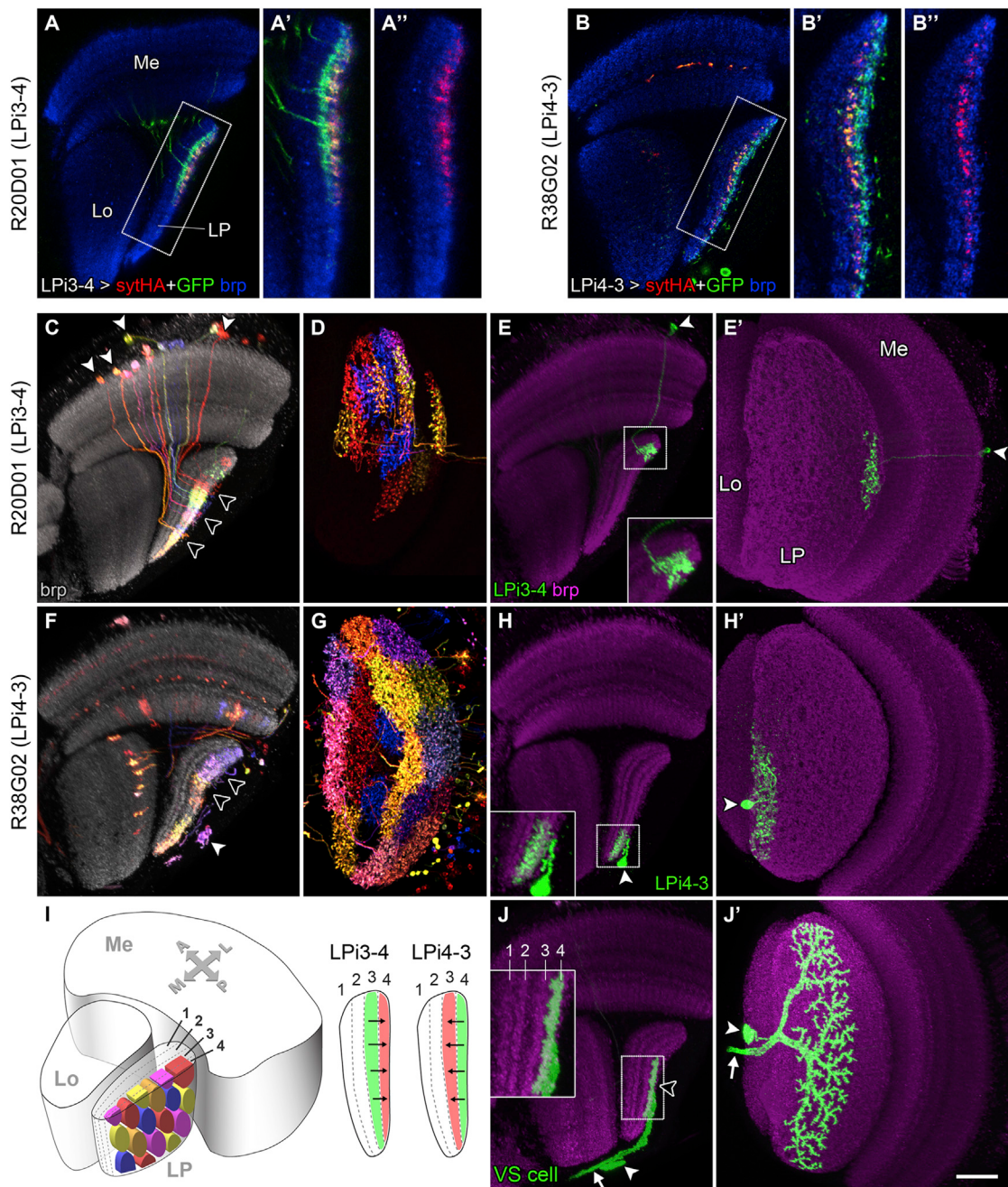


**Figure 1. Anatomical Characterization of Lobula Plate Intrinsic Neurons**

(A–B'') Co-expression of GFP and the presynaptic marker synaptotagmin by LPi-specific Gal4 driver lines (A, R20D01; B, R38G02) reveals the bi-stratified morphology and polarity of LPi neurites in lobula plate layers 3 and 4 in the horizontal confocal cross section (lateral up, anterior to the left). LPi3-4 neurons exhibit synaptic output sites only in layer 4 (A–A''), while LPi4-3 neurons (B–B'') with synaptotagmin in layer 3 show the opposite polarity. Postsynaptic sites are presumably restricted to the respective synaptotagmin-negative layers. Counterstaining with anti-bruchpilot (brp) highlights the synaptic neuropiles of the fly optic. (C–H') In two different views, stochastic multicolor labelings of LPi3-4 (C and D) and LPi4-3 neurons (F and G) are shown as well as individual neurons segmented from multicolor samples (E and H). Five stacks each with ~50 labeled cells for R38G02 and ~100 labeled cells for R20D01 were analyzed in detail. The layer positions and cell body locations were highly reproducible for each LPi type.

(I) Schematic representation of the fly optic lobe highlighting anatomical LPi neuron properties. LPi neurons cover lobula plate layers 3 and 4 in partly segregated patches. Since the lobula plate is organized in a retinotopic fashion, individual LPi neurons represent different points in visual space. Lobula plate cross-sections illustrate the inferred directed signal transfer. A, anterior; P, posterior; M, medial; L, lateral.

(J and J') Wide-field VS tangential cell segmented from a multicolor sample with its large dendrite restricted to layer 4.

Me, medulla; Lo, lobula; LP, lobula plate; white arrow heads, somata; black arrow heads, ramifications within the lobula plate; white arrows, VS cell axon. Scale bar, 20  $\mu$ m and 10  $\mu$ m for magnified views.

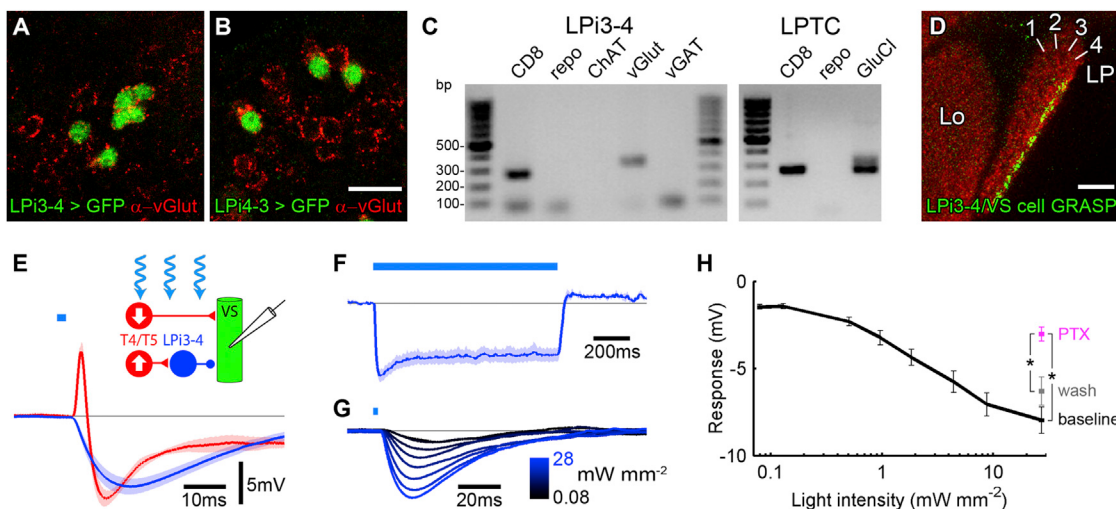


**Figure 2. LPi Neurons Provide Glutamatergic Inhibitory Input to Tangential Cells**

(A and B) Co-localization of antibodies against the vesicular glutamate transporter (vGlut) with GFP-expressing LPi neurons indicates that LPi3-4 (A) and LPi4-3 (B) both release the neurotransmitter glutamate (see also Figure S1). Scale bar, 10  $\mu$ m.

(C) Consistently, transcript profiling shows that mCD8-GFP-labeled LPi3-4 cells express vGlut (gel band with expected size of 339 bp), but neither choline acetyltransferase (ChAT) nor vesicular GABA transporter (vGAT). The bands detected in the repo and vGAT lanes do not match the predicted sizes of products from cDNA templates (137 and 151 bp, respectively) and probably correspond to primers. Transcript amplification of mCD8 and the glial marker repo were included as positive and negative control, respectively. Lobula plate tangential cells (LPTCs) express glutamate-gated chloride channel  $\alpha$  (GluCl $\alpha$ , expected size 265 bp), indicating an inhibitory synaptic connection between LPi neurons and LPTCs.

(D) GFP reconstitution across synaptic partners (GRASP) reveals contacts between LPi3-4 cells and VS tangential cells in layer 4 (see also Figure S2). Lo, lobula; LP, lobula plate. Scale bar, 20  $\mu$ m.

(E) Optogenetic activation of Channelrhodopsin-2-H134R-expressing T4/T5 cells in blind flies using a 2 ms pulse of blue light (472/30 nm,  $\sim 3$  mW mm $^{-2}$ ) leads to a biphasic excitatory/inhibitory synaptic response in VS cells (red trace, n = 4; data taken from Mauss et al., 2014). Optogenetic activation of LPi3-4 cells ( $\sim 30$  mW mm $^{-2}$ ) in contrast causes a purely inhibitory response in VS cells with a similar onset latency (blue trace, n = 7). The schematic depicts the inferred connectivity between T4/T5, LPi3-4, and VS cells supported by the data, with excitatory cholinergic and inhibitory glutamatergic synapses marked by red triangles and a blue circle, respectively.

(F) Sustained hyperpolarizing VS cell response to 1 s optogenetic LPi3-4 activation (n = 6;  $\sim 1$  mW mm $^{-2}$ ).

(G) VS cell responses to 2 ms optogenetic LPi3-4 activation with varying light intensities.

(H) Quantification of data shown in (G) as baseline-subtracted response minima. For the highest light intensity and n = 4 cells, responses were also quantified after 10 min bath perfusion with 25  $\mu$ M PTX and after another 30 min wash. Significant differences were established using a two-tailed Wilcoxon rank-sum test, with asterisk indicating p < 0.05. Data in (E) to (H) are represented as mean  $\pm$  SEM.

corresponding to a temporal frequency of 1 Hz (Figures 3E and 3F). Finally, to assess how T4/ON and T5/OFF signals are integrated by LPi cells, we imaged individual presynaptic LPi boutons in the lobula plate and stimulated flies by moving ON and OFF edges separately. Most LPi3-4 boutons showed mixed but also ON and OFF edge-selective responses (Figure 3G). In LPi4-3 cells, mixed and ON edge-selective responses dominated (Figure 3H). These results indicate that both T4 and T5 cells at least partly converge onto individual LPi cells. Taken together, the anatomical overlap between T4/T5 output and LPi cell input arbors as well as their precisely matching visual response properties strongly suggests that LPi cells receive directionally tuned excitatory inputs from T4 and T5 cells.

#### Tangential Cell Motion Responses without LPi Input

Our data so far show that LPi3-4 neurons provide inhibitory input to VS cells and depolarize to opposite motion directions. To test directly whether LPi3-4 neurons convey null direction inhibition to VS cells, we performed patch-clamp recordings from VS cells (Joesch et al., 2008) in flies with LPi3-4 neurons silenced by

expression of tetanus toxin (Sweeney et al., 1995) (Figure 4A; “block flies”: LPi3-4-Gal4 > UAS-TNT-E), as well as in parental control flies. In control flies, stimulating the eye with gratings moving in the VS cells’ preferred direction (downward) produced graded depolarizations, while null direction stimulation (upward motion) hyperpolarized VS cells (Figure 4B, black and gray traces/bars). In block flies, preferred direction responses were similar to the controls. However, in sharp contrast, null direction responses were almost entirely absent (Figure 4B, red traces/bars). VS cell responses to individual ON and OFF edges were also strongly diminished in LPi3-4 block flies selectively for null direction motion (Figure 4C).

We next aimed to determine whether LPi activity might shape preferred direction response properties in VS cells. It has been suggested that the subtraction of oppositely tuned antagonistic inputs sharpens directional tuning in postsynaptic neurons (Levick et al., 1969; Oyster et al., 1971; Sato et al., 1991; Single et al., 1997). In *Drosophila* however, this might not be a vital requirement since the directional tuning of T4/T5 cells seems already sufficiently narrow to avoid significant overlap at orthogonal

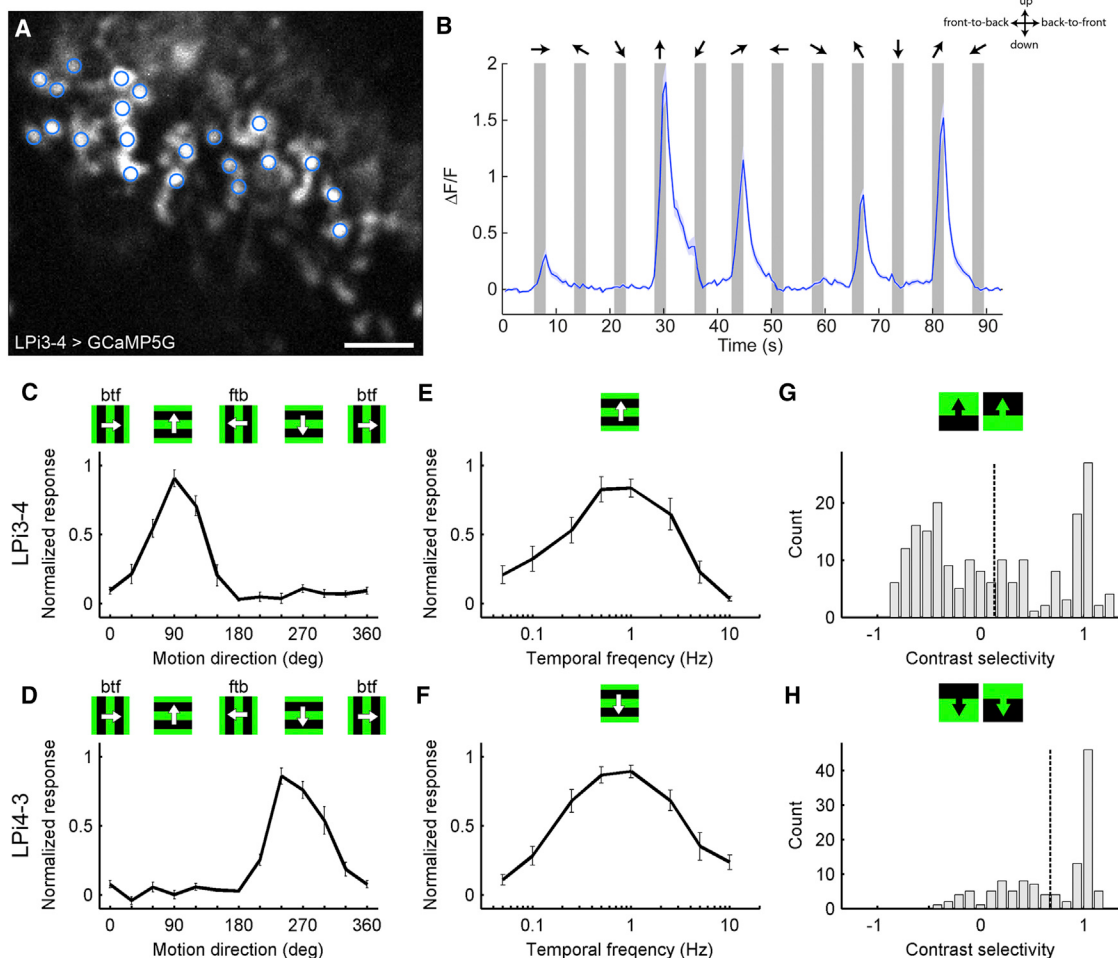


**Figure 3. LPi Neurons Are Direction Selective in Agreement with Layer-Specific Input from T4/T5 Terminals**

(A) Representative frame from a two-photon calcium imaging experiment (LPi3-4 expressing GCaMP5G) with ROIs indicated with blue circles. Scale bar, 5 μm.  
(B) Average time-varying fluorescence ( $\Delta F/F$ ) across all ROIs in response to square-wave gratings moving in the above indicated directions.  
(C and D) LPi3-4 ( $n = 7$ ) and LPi4-3 ( $n = 10$ ) neurons respond specifically to upward and downward motion, respectively (btf, back to front; ftb, front to back).  
(E and F) Both LPi cell types respond optimally to gratings moving at a temporal frequency of 1 Hz (E,  $n = 5$ ; F,  $n = 7$ ).  
(G) Individual LPi3-4 neuron boutons can show preferences for moving ON or OFF edges or mixed responses to both contrast polarities ( $n = 10$  flies,  $n = 198$  boutons).  
(H) Calcium signals from individual LPi4-3 boutons ( $n = 8$ ,  $n = 120$ ) indicate an average preference for ON over OFF edges.  
Contrast selectivity =  $(R_{ON} - R_{OFF})/(R_{ON} + R_{OFF})$ . Dashed vertical lines indicate the population mean. Data in (B) to (F) are represented as mean ± SEM.

directions (Maisak et al., 2013). We directly tested this by measuring VS cell responses in control and LPi block flies as a function of motion direction. The directional tuning curve of VS cells in control flies reveals a sinusoidal dependence on motion direction, with negative potential changes around 90° (upward) and positive potential changes around 270° (downward) (Figure 5A, black curve). Polarity and tuning width of the positive and negative parts of the curve closely match those obtained from calcium signals of T4d/T5d cells terminating in layer 4 and the inverse signals from T4c/T5c innervating layer 3 (Maisak et al., 2013), respectively, further indicating that VS cells integrate antagonistic inputs from oppositely tuned T4/T5 cells. As expected, in LPi3-4 block flies, directions around 90° on average did not evoke hyperpolarizing potential changes in VS cells (Fig-

ure 5A, red curve). The tuning curve for preferred directions around 270°, however, resembled that of the control condition. To test for a potential function in gain control, we presented gratings at different contrasts (Figure 5B). The resulting response functions showed lack of null direction inhibition selectively in LPi3-4 block flies but were indistinguishable between both experimental conditions for preferred directions. Last, we asked whether LPi input might influence the dynamics of the depolarizing VS cell responses to coherent pattern motion. To this end, we tested a dynamic motion stimulus consisting of a sine-wave grating changing velocity and direction according to a pseudo-random velocity distribution. In control flies, the VS cells' potential followed the pattern velocity with graded hyper- and depolarizations (Figures 5C–5E, black). In contrast, the responses in LPi

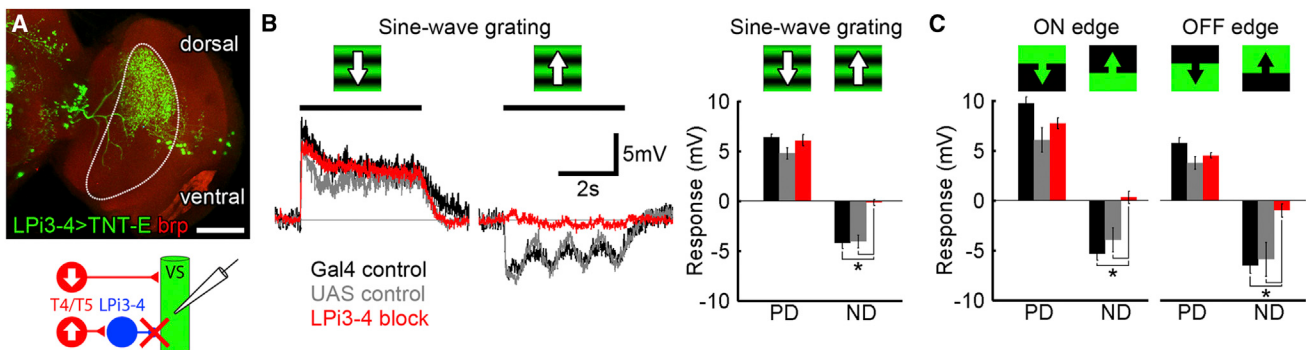


**Figure 4. LPi Neurons Convey Null Direction Responses to Tangential Cells**

(A) Tetanus toxin light chain (TNT-E) is expressed in LPi3-4 neurons to silence synaptic release. Since expression by the driver line is confined to the dorsal part of the lobula plate (demarcated by white line), visual stimuli to test LPi3-4 function were partly confined to the upper half of the visual field. Scale bar, 50  $\mu$ m. The schematic depicts the experimental approach to probe LPi3-4 cell function by whole-cell voltage recordings from VS cells.

(B) Visual stimulation of flies with sine-wave gratings moving down (preferred direction [PD]) or up (null direction [ND]) evokes de- and hyperpolarization in control flies (Gal4, n = 9; UAS, n = 5). In LPi3-4 block flies (n = 10), hyperpolarizing responses to ND motion are selectively abolished. Voltage traces represent averaged data, with SEM omitted for clarity.

(C) VS cell responses to moving ON and OFF edges are similarly affected with ND responses to both edge contrasts abolished in LPi3-4 block flies (Gal4, n = 9; UAS n = 4; LPi3-4 block, n = 10).

Significant differences were established using a two-tailed Wilcoxon rank-sum test, with asterisk indicating  $p < 0.0001$ . Data are represented as mean  $\pm$  SEM.

block flies were largely clipped for negative velocities (upward motion), while positive velocities (downward motion) were still encoded in membrane depolarizations with no obviously different dynamics (Figures 5C–5E, red).

Taken together, these data demonstrate that LPi3-4 neurons integrate direction-selective information from T4 and T5 cells in lobula plate layer 3 and convey this information to VS cells via inhibitory synapses in layer 4, giving rise to the VS cells' null direction responses. However, the absence of inhibitory LPi3-4 input does not noticeably alter the direction tuning, gain, or dynamics of the remaining depolarizing tangential cell potential changes in response to coherently moving patterns (Figures 4, 5, and S3).

#### Functional Implications of Motion Opponency

Since tangential cell dendrites—the postsynaptic targets of LPi neurons—integrate inputs over large receptive fields (Figure 1J'), we reasoned that motion opponency might serve to cancel out incoherent motion signals impinging on different parts of the dendritic tree. To test this, we devised three visual stimuli containing opponent motion information (Figures 6A–6C): (1) 100 dots with random motion trajectories, reflecting independent object motion ("motion noise"); (2) a radially expanding pattern simulating flight through a tunnel ("expanding flow"); and (3) an expanding black square as perceived during object approach on a collision course ("looming square"). We presented these patterns to control and LPi block flies while recording from VS cells. Average responses in control flies were consistently subtle for all patterns (Figures 6D–6G, black traces and bars). In contrast, VS cells in LPi block flies showed robust depolarizations (Figures 6D–6G, red traces and bars). These differences were largely captured by model simulations of a motion detection circuit (for details, see *Supplemental Experimental Procedures*) subjected to the same kind of stimuli (Figures 6H–6J). We therefore conclude that, in the absence of motion opponent

inhibition, VS cells are rendered sensitive to incoherent motion signals and that the integration of motion opponent inputs serves to reduce noise sensitivity and to increase flow-field selectivity in wide-field neurons.

#### DISCUSSION

Motion detection is a fundamental function of all higher visual systems. It is a paradigmatic model for sensory feature extraction since motion information is not explicitly encoded in the single receptor response but has to be computed by downstream neural circuits. Motion detection can be described as a two-stage process (Borst and Egelhaaf, 1990; Egelhaaf et al., 1989; Reichardt, 1987; van Santen and Sperling, 1985): In the first stage, direction-selective signals are generated by correlating the output from neighboring photoreceptors after asymmetric temporal filtering. Neural substrates corresponding to these correlators are, for instance, the T4/T5 cells of the fly optic lobes (Maisak et al., 2013) and the dendrites of starburst amacrine cells in the mammalian retina (Euler et al., 2002; Kim et al., 2014). In the second stage, signals from oppositely tuned correlators are subtracted from each other, giving rise to a fully opponent output. This processing step is implemented in the fly optic lobe on the dendrites of the lobula plate tangential cells (Borst et al., 1995; Joesch et al., 2008), which receive two kinds of inputs: (1) a direct excitatory input from T4/T5 cells terminating within the same lobula plate layer, giving rise to depolarization during preferred direction motion (Maisak et al., 2013; Mauss et al., 2014; Schnell et al., 2012); and (2) as shown here, an indirect inhibitory input via bi-stratified LPi neurons from T4/T5 cells terminating in the adjacent layer, causing hyperpolarization during null direction motion (Figure 7).

GABAergic inhibition has been shown to shape response properties of interneurons in early visual processing by mediating lateral antagonistic effects in *Drosophila* (Freifeld et al.,

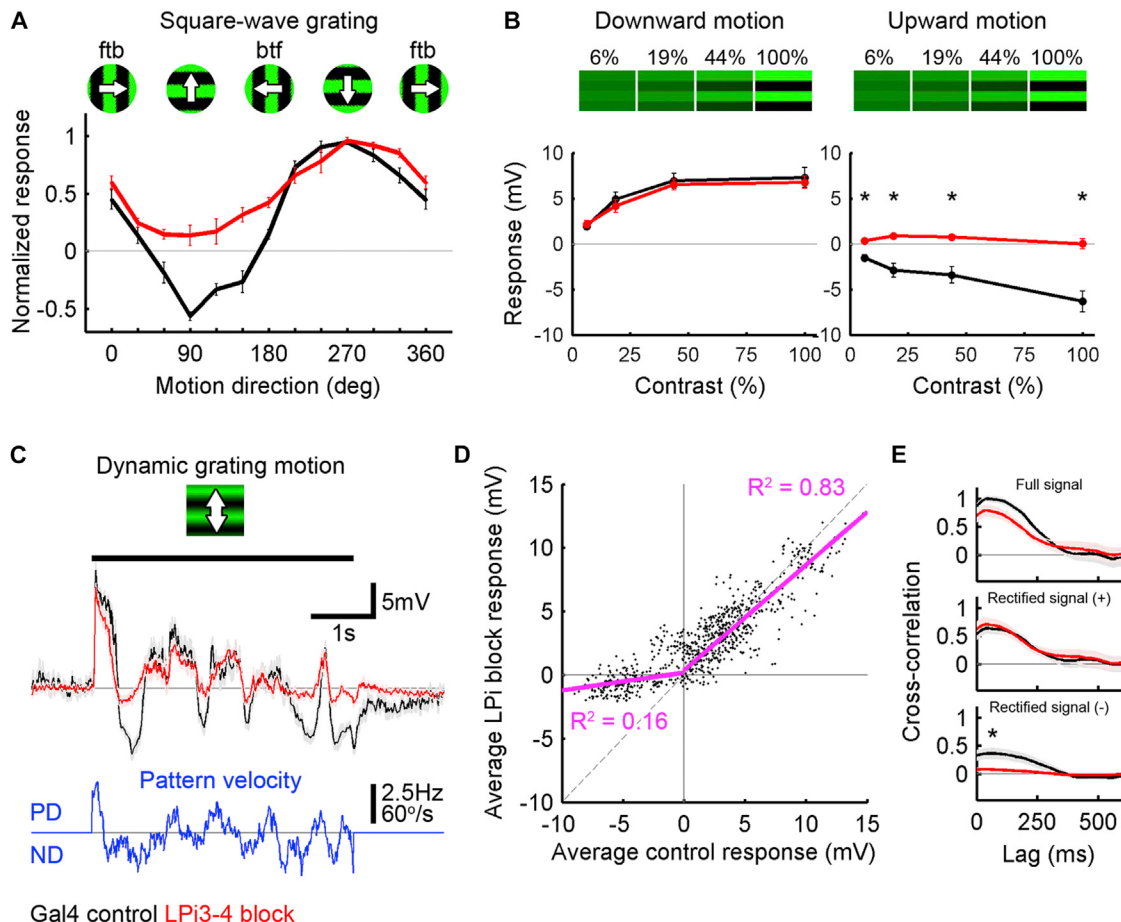


**Figure 5. Directional Tuning, Gain, and Dynamics of Preferred Direction Responses to Coherent Wide-Field Motion Are Normal in Absence of LPi Input**

(A) The directional tuning curve of VS cells in control flies ( $n = 6$ ) shows a sinusoidal dependence on motion direction. Blocking LPi3-4 neurons ( $n = 6$ ) selectively clips all hyperpolarizing responses. ftb, front to back; btf, back to front.

(B) Preferred direction excitation as a function of pattern contrast is indistinguishable between control ( $n = 7$ ) and LPi3-4 block conditions ( $n = 7$ ). Null direction inhibition is selectivity abolished for all contrasts in absence of LPi3-4 activity.

(C) Averaged VS cell voltage responses to sine-wave gratings dynamically moving up and down with velocities following a pseudo-random temporal profile (blue, upward deflection represents downward motion). While the voltage responses in VS cells in control flies (black,  $n = 7$ ) followed the velocity in both directions, the VS cell membrane voltage in LPi3-4 block flies (red,  $n = 6$ ) predominantly encoded PD (downward) motions.

(D) Scatter plot of average membrane voltage from VS cells in LPi block against control flies obtained from dynamic motion stimulation (blue trace in C; played forward and backward). For positive control values, the distribution follows a positive linear relationship well described by  $y = 0.83x + 0.35$  ( $R^2 = 0.83$ ), revealing little differences between the two conditions. For negative control values, this relationship breaks down ( $y = 0.14x + 0.17$ ;  $R^2 = 0.16$ ), due to the clipped hyperpolarizing responses in LPi block flies.

(E) Cross-correlation of full, positively, and negatively rectified control and LPi block VS cell signals with the velocity profile of the dynamic motion stimulus (blue trace in C; played forward and backward). Peak correlation for negatively rectified signals is significantly smaller in LPi block compared to control flies since hyperpolarizing potentials are largely missing in the absence of LPi input. For the positively rectified signals, no significant difference is observed. Hence, the lack of inhibitory LPi3-4 input to VS cells does not alter the dynamics of their depolarizing responses.

Significant differences were established using a two-tailed Wilcoxon rank-sum test, with asterisk indicating  $p < 0.001$ . Data are represented as mean  $\pm$  SEM. See also Figure S3.

2013). Work in the *Calliphora* visual system has ascribed a more specialized role for GABAergic transmission in mediating null direction inhibition, based on experiments using picrotoxinin as a GABA receptor antagonist (Brotz and Borst, 1996; Egelhaaf et al., 1990). Unexpectedly, in the same context, we have identified glutamate as the underlying neurotransmitter in *Drosophila*. This discrepancy is perhaps due to neglecting the action of the

pharmacologic compound as a rather unspecific chloride channel blocker (Liu and Wilson, 2013; Marder and Paupardin-Tritsch, 1978; Mauss et al., 2014) in earlier work. It should also be noted that, in *Calliphora*, picrotoxinin application was shown to have two effects on tangential cell motion processing: preferred direction depolarization was enlarged, and null direction hyperpolarization was replaced by noticeable depolarization

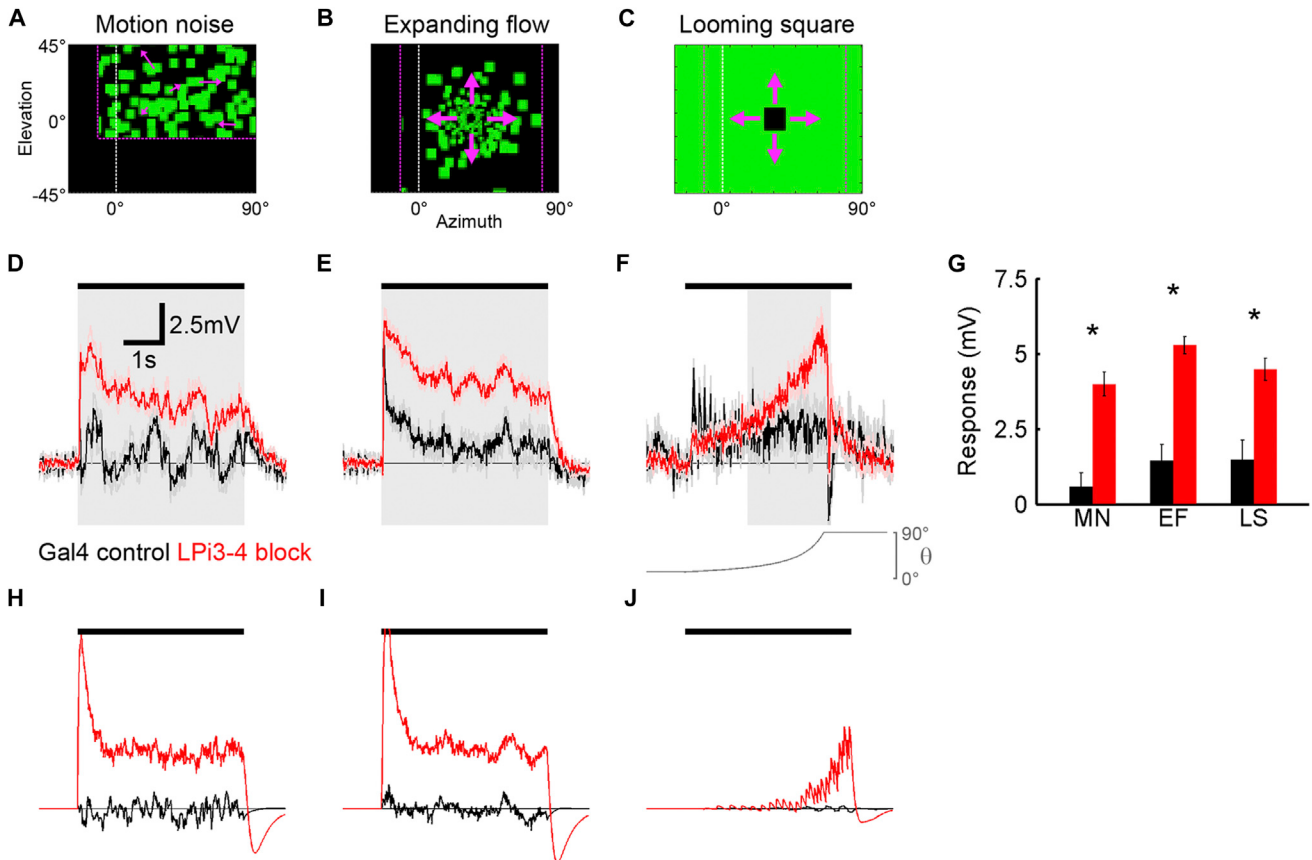


**Figure 6. Silencing Inhibitory Motion-Opponent Input to Tangential Cells Increases Responses to Motion Noise and Non-uniform Flow-Field Patterns**

(A–C) Stimulation arena showing images from visual patterns used to probe VS cell responses in control and LPi3-4 block flies. Independent motion of 100 dots following random two-dimensional trajectories (A); expanding flow field simulating flight through a tunnel (B); and looming black square (C) with angular size as a function of time shown in (F).

(D–F) Averaged recording traces ( $n = 6$ ) from Gal4 control (black) and LPi3-4 block (red) flies subjected to the above shown visual patterns (four independent patterns for each D and E).

(G) Bars represent average baseline-subtracted responses. Shaded gray areas in (D) to (F) demarcate the response time window used for quantification. VS cell responses in control flies were small for all stimuli with average depolarizations of  $< 1.5$  mV. In contrast, VS cells without motion-opponent inhibitory input (LPi block flies) showed significantly higher depolarizations ( $> 4$  mV).

(H to J) Tangential cell responses could be largely captured by a computational model incorporating spatial integration of elementary motion detectors with and without motion-opponent subtraction (see [Supplemental Experimental Procedures](#) for details).

Significant differences were established using a two-tailed Wilcoxon rank-sum test, with asterisk indicating  $p < 0.005$ . Data are represented as mean  $\pm$  SEM.

(Single et al., 1997). This was interpreted as evidence for weak directional tuning of the inputs, i.e., the later identified T4/T5 cells. A similar result was observed in *Drosophila* (A.S.M., unpublished data). The LPi3-4 block in *Drosophila*, however, did not produce a prominent null direction depolarization, and preferred direction excitation was indistinguishable from the control condition (Figures 4, 5, and S3). Since a recent study demonstrated narrow directional tuning of the T4/T5 cells (Maisak et al., 2013), rendering postsynaptic directional response sharpening unnecessary, we suggest that picrotoxinin off-target effects on glutamate or GABA receptors in the upstream circuit are responsible for this inconsistency, and genetic LPi block represents a more suitable approach to eliminate null direction inhibition.

We have focused our analysis on the LPi3-4 neurons and their postsynaptic partners in layer 4, the VS cells, because of their

experimental accessibility. However, our findings can be most likely extended to the other layers. Tangential cells with dendrites in layer 3 have been identified in other fly species (Hausen, 1976, 1984; Wertz et al., 2008). Such so-called V2 cells are motion opponent with preference to upward flow, in agreement with their presumed inputs from excitatory layer 3 T4/T5 cells. Since our data indicate that the LPi4-3 neurons convey glutamatergic signals selective for downward motion to lobula plate layer 3, it seems plausible that a motion-opponent wiring complementary to the LPi3-4/VS cell connectivity exists as well (Figure 7). The preference of LPi4-3 cells to ON over OFF edges is unexpected because in contrast to tangential cells, LPi4-3 neurons appear to be able to differentiate between T4/ON and T5/OFF input. Whether this finding hints toward an ON-selective null direction inhibition in layer 3 postsynaptic cells, perhaps dictated by

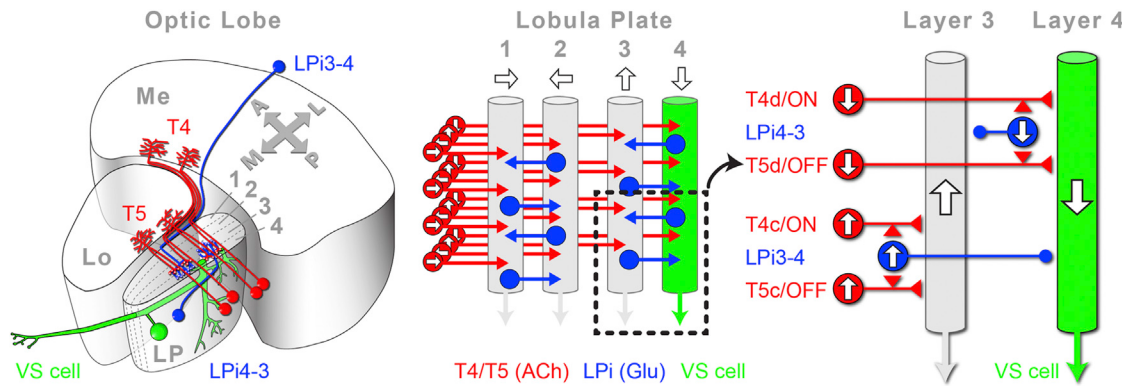


**Figure 7. Connectivity Model of the Lobula Plate**

Four subclasses of T4 and T5 cells (red) convey ON and OFF direction-selective input to the lobula plate. Both T4 and T5 cells signal front-to-back, back-to-front, upward, and downward motion and project according to their tuning to layers 1–4 (those encoding horizontal motion and targeting layers 1 and 2 are depicted only in the middle schematic for clarity). Lobula plate tangential cells (green) of the vertical system (VS) extend their dendrites in lobula plate layer 4, where they receive direct excitatory inputs from T4/T5 cells tuned to downward motion. In addition, LPI4-3 neurons (blue) obtain excitatory T4/T5 input during upward motion in layer 3 and convey a sign-inverted signal onto VS cells in the adjacent layer via an inhibitory glutamatergic synapse. This arrangement generates a fully motion-opponent response in VS cells. LPI4-3 neurons likely contribute to a complementary circuit in the other direction. Additional LPi neurons are postulated to constitute a corresponding motion-opponent circuit for the horizontal system tangential cells in layers 1 and 2. A, anterior; P, posterior; M, medial; L, lateral.

certain natural stimulus statistics, or whether it reflects merely a bias of the driver line for an ON-selective LPI4-3 subgroup remains to be investigated. Some presynaptic swellings of the complementary LPI3-4 cells also exhibited polarity preference, but at present, it is unclear whether this indicates a similar T4/T5 selectivity on a cell-by-cell basis or stochastic sampling of inputs. The functional architecture of lobula plate layers 1 and 2 strongly resembles the one of layers 3 and 4 with a 90° directional tuning shift (Figure 7): motion-opponent HS cells with a preference for front-to-back motion ramify their dendrites exclusively in layer 1 (Schnell et al., 2010), while motion-opponent Hx cells that prefer back-to-front motion confine their dendrites to layer 2 (Wasserman et al., 2015). We therefore anticipate the existence of at least two complementary horizontal LPi cell types in those layers too. It thus seems that global motion information is processed initially in two segregated horizontal and vertical subsystems with little direct interaction. Rather than representing the cardinal directions in a clock- or counter-clockwise manner, the four lobula plate layers are arranged such that opposite directions are represented side by side. This functional organization might serve to facilitate efficient nearest-neighbor interactions of motion-opponent signals.

Similar to the fly lobula plate, the dorsal lateral geniculate nucleus (dLGN) in mammals relays direction-selective signals from the retina to higher brain centers (Cruz-Martin et al., 2014). Some fundamental parallels in the organization of the two brain regions seem to exist. Their input channels, T4/T5 neurons in flies and ON/OFF direction-selective ganglion cells in mammals, predominantly encode the four cardinal directions of motion up, down, left, and right (Maisak et al., 2013; Piscopo et al., 2013). The anatomical separation of the vertical and horizontal subsystems in flies seems to be mirrored, at least to a degree, in the dLGN, where opposing horizontal direction information resides in the superficial region of mouse dLGN, segregated from vertical motion (Marshel et al., 2012). Moreover, a feed-forward inhibitory

principle to generate motion opponency that we describe in the fly might also prevail in the dLGN, where directionally selective output neurons were suggested to integrate opposing signals from retinal ganglion cells (Levick et al., 1969; Oyster et al., 1971), possibly directly and indirectly via local inhibitory neurons (Cox et al., 1998; Singer, 1977; Wang et al., 2011). However, many mammalian dLGN neurons are also orientation selective, potentially obtaining this property by integrating opponent excitatory direction-selective input (Cruz-Martin et al., 2014; Marshel et al., 2012; Piscopo et al., 2013).

Associated with their proposed role as matched filters for sensing the optic flow generated by an animal's self-motion, in contrast to dLGN neurons, lobula plate tangential cells have large receptive fields, in some cases covering more than 100 degrees of visual space (Hopp et al., 2014; Joesch et al., 2008; Krapp and Hengstenberg, 1996; Schnell et al., 2010). Independent movement, e.g., originating from conspecifics or foliage, thus poses a challenge to the system by providing excitatory drive to tangential cells not associated with self-motion. Our experiments with intact and silenced LPi neurons support the idea that such inputs are attenuated by antagonistic signals from oppositely moving objects elsewhere in the visual scene (Figure 6D). Perhaps more importantly, different flight maneuvers generate ambiguous optic flow patterns in sub-parts of the receptive field. For instance, both lift and forward translation cause downward optic flow in the ventral visual field, while only the latter produces upward flow dorsally. Taking into account excitation only, a reliable distinction between those patterns, especially under varying stimulus intensities, i.e., contrasts as experienced in natural scenes, seems inconceivable. We have demonstrated (Figures 6E and 6F) that LPi cells strongly reduce such ambiguities, most likely by cancelling the excitation caused in one part of the dendrite by inhibition in another part. Motion opponency is thus reminiscent of other neural opponent mechanisms. In the classical example of color opponency, neural comparison discriminates

sensory signals that are ambiguous at the level of photoreceptors in terms of wavelength and stimulus intensity. Notably, while color vision requires at least two separate measurements at any point in space, motion opponency disambiguates different optic flow-fields derived from the same photoreceptor responses. Given that wide-field motion-sensitive neurons in various other systems are also motion opponent (Collett and Blest, 1966; Duffy and Wurtz, 1991; Ibbotson, 1991; Wylie et al., 1998), we suggest that such a mechanism might be universally required to increase sensitivity and selectivity for optic flow-fields associated with self-motion. Similar neural comparators might be widely used for the extraction of equally complex sensory features.

## EXPERIMENTAL PROCEDURES

### Flies

Details about all fly stocks and genotypes can be found in the [Supplemental Experimental Procedures](#).

### Immunostaining

Brains were dissected in phosphate-buffered saline and were fixed in 4% PFA with 0.1% TritonX or, for anti-vGlut and anti-GAD1, with Bouin's fixative. Brains were subsequently washed and sequentially stained with primary and fluorophore-conjugated secondary antibodies. 2% normal goat serum was added to all primary and secondary antibody solutions. Brains were optically sectioned with a Leica TCS SP5 confocal microscope. Brains expressing GRASP components were fixed and stained against the neuropile marker bruchpilot. Afterward, native GRASP fluorescence was visualized. For more details, please refer to the [Supplemental Experimental Procedures](#).

### Multicolor Stochastic Labeling

Stochastic single-cell labeling was carried out using "MultiColor FlipOut" (MCFO) (Nern et al., 2015), a multicolor adaptation of the "flip-out" approach (Struhl and Basler, 1993).

### Transcript Profiling

The transcript profiling protocol was modified from the method described previously (Takemura et al., 2011). For details, please see the [Supplemental Experimental Procedures](#), Table S1, and Figure S4.

### Two-Photon Calcium Imaging

Two-photon imaging was performed on a custom-built microscope, as previously described (Maisak et al., 2013). Images were acquired at a frame rate of 1.88 Hz.

### Electrophysiology, Optogenetic Stimulation, and Pharmacology

Electrophysiological and optogenetic experiments were performed as described previously (Mauss et al., 2014). Picrotoxinin (PTX; Sigma P8390) was dissolved in dimethylsulfoxide at 50 mM and was kept as a stock at -20°C. For experiments, PTX was diluted in external solution to 25 μM and washed in (10 min) and out (30 min) at 2 ml/min.

### Visual Stimulation

Custom-built LED arenas were used for visual stimulation in calcium imaging and electrophysiology experiments. The arenas covered ~170° and 90° in azimuth and elevation, respectively, and allowed refresh rates of 550 Hz and 16 intensity levels (Maisak et al., 2013). Identical visual stimuli were presented in three to five trials in every experiment, usually in a randomized sequence. Please refer to the [Supplemental Experimental Procedures](#) for more details.

### Physiological Data Analysis

Data from VS cell recordings and LPi calcium imaging experiments were evaluated using custom-written analysis scripts in Matlab. Details can be found in the [Supplemental Experimental Procedures](#).

### Modeling

Stimuli were calculated at 1° spatial and 10 ms temporal resolution. Every stimulus frame was convolved with a radial Gaussian function of 5° half-width and down-sampled to an array of 40 × 40 photoreceptors, corresponding to an angular separation of 5° between neighboring receptors. Please see the [Supplemental Experimental Procedures](#) for detailed parameters of the model.

## SUPPLEMENTAL INFORMATION

**Supplemental Information** includes Supplemental Experimental Procedures, four figures, and one table and can be found with this article online at <http://dx.doi.org/10.1016/j.cell.2015.06.035>.

## AUTHOR CONTRIBUTIONS

A.S.M. performed and analyzed electrophysiological recordings. K.P. carried out and analyzed immunostainings (except multicolor labeling and TNT-E expression), transcript profiling, and GRASP experiments. A.A. performed and analyzed two-photon calcium imaging experiments. A.B. did computer simulations. G.M.R. and A.N. generated the LPi driver lines and performed multicolor stochastic labeling. A.S.M. and A.B. designed the study. A.S.M., A.A., and A.B. wrote the paper with the help of all authors.

## ACKNOWLEDGMENTS

We would like to thank Barry Dickson (Janelia) for sharing unpublished fly lines; Matthias Meier, Etienne Serbe, and Jürgen Haag for help with two-photon calcium imaging; Christoph Kapfer for advice on fixation procedures; Georg Ammer and Wolfgang Essbauer for tetanus toxin staining; Aljoscha Leonhardt, Armin Bahl, and Tabea Schilling for experimental help; Wolfgang Essbauer, Christian Theile, Michael Sauter, and Renate Gleich for technical assistance; and Jürgen Haag for critically reading the manuscript. We thank the Janelia Fly-Light Project Team (especially Jennifer Jeter) for assistance with MCFO sample preparation and imaging. We would also like to acknowledge Karin Nordström (Uppsala University) for sharing unpublished results. We acknowledge the Developmental Studies Hybridoma Bank for antibodies and the Bloomington Drosophila Stock Center for flies. A.A. was funded by an EMBO Long-Term Fellowship. This work was supported by the Max-Planck-Society, the Deutsche Forschungsgemeinschaft (CRC 870), and HHMI.

Received: January 13, 2015

Revised: April 1, 2015

Accepted: May 18, 2015

Published: July 16, 2015

## REFERENCES

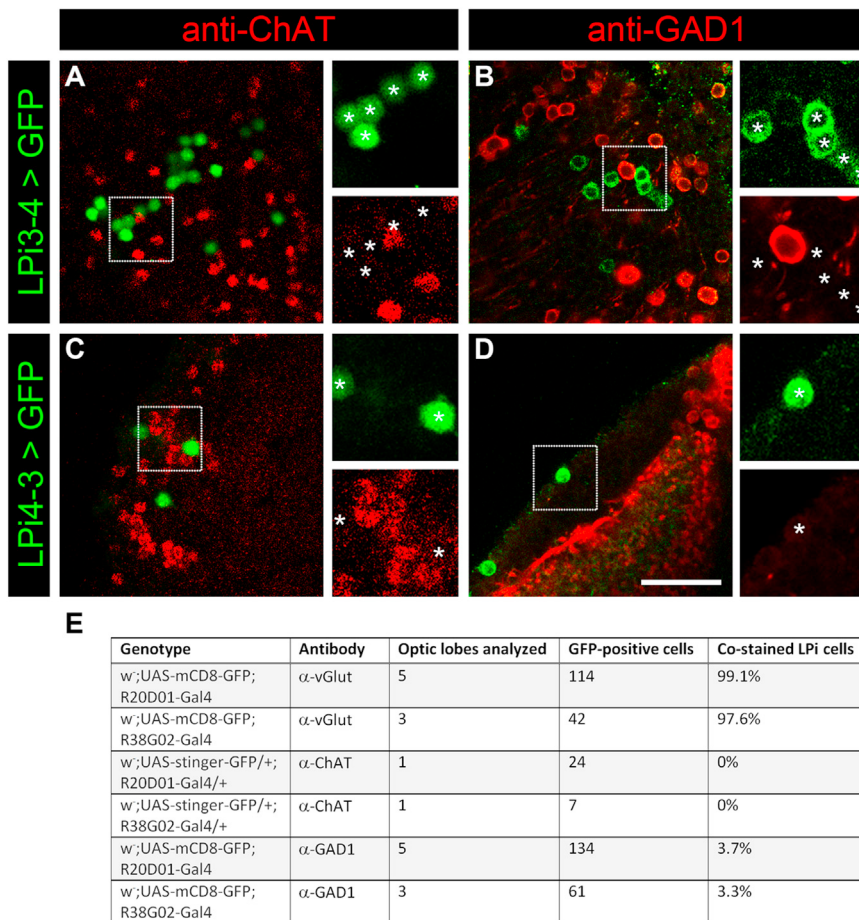
- Akerboom, J., Chen, T.-W., Wardill, T.J., Tian, L., Marvin, J.S., Mutlu, S., Calderón, N.C., Esposti, F., Borghuis, B.G., Sun, X.R., et al. (2012). Optimization of a GCaMP calcium indicator for neural activity imaging. *J. Neurosci.* 32, 13819–13840.
- Bahl, A., Ammer, G., Schilling, T., and Borst, A. (2013). Object tracking in motion-blind flies. *Nat. Neurosci.* 16, 730–738.
- Bausenwein, B., and Fischbach, K.F. (1992). Activity labeling patterns in the medulla of *Drosophila melanogaster* caused by motion stimuli. *Cell Tissue Res.* 270, 25–35.
- Bausenwein, B., Dittrich, A.P., and Fischbach, K.F. (1992). The optic lobe of *Drosophila melanogaster*. II. Sorting of retinotopic pathways in the medulla. *Cell Tissue Res.* 267, 17–28.
- Borst, A., and Egelhaaf, M. (1990). Direction selectivity of blowfly motion-sensitive neurons is computed in a two-stage process. *Proc. Natl. Acad. Sci. USA* 87, 9363–9367.
- Borst, A., Egelhaaf, M., and Haag, J. (1995). Mechanisms of dendritic integration underlying gain control in fly motion-sensitive interneurons. *J. Comput. Neurosci.* 2, 5–18.

- Borst, A., Haag, J., and Reiff, D.F. (2010). Fly motion vision. *Annu. Rev. Neurosci.* 33, 49–70.
- Brotz, T.M., and Borst, A. (1996). Cholinergic and GABAergic receptors on fly tangential cells and their role in visual motion detection. *J. Neurophysiol.* 76, 1786–1799.
- Clark, D.A., Bursztyn, L., Horowitz, M.A., Schnitzer, M.J., and Clandinin, T.R. (2011). Defining the computational structure of the motion detector in *Drosophila*. *Neuron* 70, 1165–1177.
- Collett, T.S., and Blest, A.D. (1966). Binocular, directionally selective neurones, possibly involved in the optomotor response of insects. *Nature* 212, 1330–1333.
- Cox, C.L., Zhou, Q., and Sherman, S.M. (1998). Glutamate locally activates dendritic outputs of thalamic interneurons. *Nature* 394, 478–482.
- Cruz-Martín, A., El-Danaf, R.N., Osakada, F., Sriram, B., Dhanda, O.S., Nguyen, P.L., Callaway, E.M., Ghosh, A., and Huberman, A.D. (2014). A dedicated circuit links direction-selective retinal ganglion cells to the primary visual cortex. *Nature* 507, 358–361.
- Denk, W., Strickler, J.H., and Webb, W.W. (1990). Two-photon laser scanning fluorescence microscopy. *Science* 248, 73–76.
- Duffy, C.J., and Wurtz, R.H. (1991). Sensitivity of MST neurons to optic flow stimuli. I. A continuum of response selectivity to large-field stimuli. *J. Neurophysiol.* 65, 1329–1345.
- Egelhaaf, M., Borst, A., and Reichardt, W. (1989). Computational structure of a biological motion-detection system as revealed by local detector analysis in the fly's nervous system. *J. Opt. Soc. Am. A* 6, 1070–1087.
- Egelhaaf, M., Borst, A., and Pilz, B. (1990). The role of GABA in detecting visual motion. *Brain Res.* 509, 156–160.
- Eichner, H., Joesch, M., Schnell, B., Reiff, D.F., and Borst, A. (2011). Internal structure of the fly elementary motion detector. *Neuron* 70, 1155–1164.
- Euler, T., Detwiler, P.B., and Denk, W. (2002). Directionally selective calcium signals in dendrites of starburst amacrine cells. *Nature* 418, 845–852.
- Feinberg, E.H., Vanhoven, M.K., Bendesky, A., Wang, G., Fetter, R.D., Shen, K., and Bargmann, C.I. (2008). GFP Reconstitution Across Synaptic Partners (GRASP) defines cell contacts and synapses in living nervous systems. *Neuron* 57, 353–363.
- Freifeld, L., Clark, D.A., Schnitzer, M.J., Horowitz, M.A., and Clandinin, T.R. (2013). GABAergic lateral interactions tune the early stages of visual processing in *Drosophila*. *Neuron* 78, 1075–1089.
- Hausen, K. (1976). Functional characterization and anatomical identification of motion sensitive neurons in the lobula plate of the blowfly *Calliphora erythrocephala*. *Z. Naturforsch. C* 31, 629–633.
- Hausen, K. (1984). The lobula-complex of the fly: Structure, function and significance in visual behaviour. *Photoreception and Vision in Invertebrates* 74, 523–559.
- Hausen, K., Wolburg-Buchholz, W., and Ribi, W.A. (1980). The synaptic organization of visual interneurons in the lobula complex of flies. A light and electron microscopical study using silver-intensified cobalt-impregnations. *Cell Tissue Res.* 208, 371–387.
- Hopp, E., Borst, A., and Haag, J. (2014). Subcellular mapping of dendritic activity in optic flow processing neurons. *J. Comp. Physiol. A Neuroethol. Sens. Neural Behav. Physiol.* 200, 359–370.
- Ibbotson, M.R. (1991). Wide-field motion-sensitive neurons tuned to horizontal movement in the honeybee, *Apis mellifera*. *J. Comp. Physiol. A* 168, 91–102.
- Jenett, A., Rubin, G.M., Ngo, T.T., Shepherd, D., Murphy, C., Dionne, H., Pfeiffer, B.D., Cavallaro, A., Hall, D., Jeter, J., et al. (2012). A GAL4-driver line resource for *Drosophila* neurobiology. *Cell Rep* 2, 991–1001.
- Joesch, M., Plett, J., Borst, A., and Reiff, D.F. (2008). Response properties of motion-sensitive visual interneurons in the lobula plate of *Drosophila melanogaster*. *Curr. Biol.* 18, 368–374.
- Joesch, M., Schnell, B., Raghu, S.V., Reiff, D.F., and Borst, A. (2010). ON and OFF pathways in *Drosophila* motion vision. *Nature* 468, 300–304.
- Joesch, M., Weber, F., Eichner, H., and Borst, A. (2013). Functional specialization of parallel motion detection circuits in the fly. *J. Neurosci.* 33, 902–905.
- Kim, J.S., Greene, M.J., Zlateski, A., Lee, K., Richardson, M., Turaga, S.C., Purcaro, M., Balkam, M., Robinson, A., Behabadi, B.F., et al.; EyeWirers (2014). Space-time wiring specificity supports direction selectivity in the retina. *Nature* 509, 331–336.
- Krapp, H.G., and Hengstenberg, R. (1996). Estimation of self-motion by optic flow processing in single visual interneurons. *Nature* 384, 463–466.
- Levick, W.R., Oyster, C.W., and Takahashi, E. (1969). Rabbit lateral geniculate nucleus: sharpener of directional information. *Science* 165, 712–714.
- Liu, W.W., and Wilson, R.I. (2013). Glutamate is an inhibitory neurotransmitter in the *Drosophila* olfactory system. *Proc. Natl. Acad. Sci. USA* 110, 10294–10299.
- Maisak, M.S., Haag, J., Ammer, G., Serbe, E., Meier, M., Leonhardt, A., Schilling, T., Bahl, A., Rubin, G.M., Nern, A., et al. (2013). A directional tuning map of *Drosophila* elementary motion detectors. *Nature* 500, 212–216.
- Marder, E., and Paupardin-Tritsch, D. (1978). The pharmacological properties of some crustacean neuronal acetylcholine, gamma-aminobutyric acid, and L-glutamate responses. *J. Physiol.* 280, 213–236.
- Marshel, J.H., Kaye, A.P., Nauhaus, I., and Callaway, E.M. (2012). Anterior-posterior direction opponency in the superficial mouse lateral geniculate nucleus. *Neuron* 76, 713–720.
- Mauss, A.S., Meier, M., Serbe, E., and Borst, A. (2014). Optogenetic and pharmacologic dissection of feedforward inhibition in *Drosophila* motion vision. *J. Neurosci.* 34, 2254–2263.
- Nern, A., Pfeiffer, B.D., and Rubin, G.M. (2015). Optimized tools for multicolor stochastic labeling reveal diverse stereotyped cell arrangements in the fly visual system. *Proc. Natl. Acad. Sci. USA* 112, E2967–E2976.
- Oyster, C.W., Takahashi, E., and Levick, W.R. (1971). Information processing in the rabbit visual system. *Doc. Ophthalmol.* 30, 161–204.
- Pfeiffer, B.D., Jenett, A., Hammonds, A.S., Ngo, T.-T.B., Misra, S., Murphy, C., Scully, A., Carlson, J.W., Wan, K.H., Laverty, T.R., et al. (2008). Tools for neuroanatomy and neurogenetics in *Drosophila*. *Proc. Natl. Acad. Sci. USA* 105, 9715–9720.
- Piscopo, D.M., El-Danaf, R.N., Huberman, A.D., and Niell, C.M. (2013). Diverse visual features encoded in mouse lateral geniculate nucleus. *J. Neurosci.* 33, 4642–4656.
- Reichardt, W. (1987). Evaluation of optical motion information by movement detectors. *J. Comp. Physiol. A Neuroethol. Sens. Neural Behav. Physiol.* 161, 533–547.
- Reiff, D.F., Plett, J., Mank, M., Griesbeck, O., and Borst, A. (2010). Visualizing retinotopic half-wave rectified input to the motion detection circuitry of *Drosophila*. *Nat. Neurosci.* 13, 973–978.
- Rister, J., Pauls, D., Schnell, B., Ting, C.Y., Lee, C.H., Sinakevitch, I., Morante, J., Strausfeld, N.J., Ito, K., and Heisenberg, M. (2007). Dissection of the peripheral motion channel in the visual system of *Drosophila melanogaster*. *Neuron* 56, 155–170.
- Sato, H., Daw, N.W., and Fox, K. (1991). An intracellular recording study of stimulus-specific response properties in cat area 17. *Brain Res.* 544, 156–161.
- Schnell, B., Joesch, M., Forstner, F., Raghu, S.V., Otsuna, H., Ito, K., Borst, A., and Reiff, D.F. (2010). Processing of horizontal optic flow in three visual interneurons of the *Drosophila* brain. *J. Neurophysiol.* 103, 1646–1657.
- Schnell, B., Raghu, S.V., Nern, A., and Borst, A. (2012). Columnar cells necessary for motion responses of wide-field visual interneurons in *Drosophila*. *J. Comp. Physiol. A Neuroethol. Sens. Neural Behav. Physiol.* 198, 389–395.
- Scott, E.K., Raabe, T., and Luo, L. (2002). Structure of the vertical and horizontal system neurons of the lobula plate in *Drosophila*. *J. Comp. Neurol.* 454, 470–481.
- Shinomiya, K., Karuppudurai, T., Lin, T.Y., Lu, Z., Lee, C.H., and Meinertzhagen, I.A. (2014). Candidate neural substrates for off-edge motion detection in *Drosophila*. *Curr. Biol.* 24, 1062–1070.

- Silkes, M., Gohl, D.M., Fisher, Y.E., Freifeld, L., Clark, D.A., and Clandinin, T.R. (2013). Modular use of peripheral input channels tunes motion-detecting circuitry. *Neuron* 79, 111–127.
- Singer, W. (1977). Control of thalamic transmission by corticofugal and ascending reticular pathways in the visual system. *Physiol. Rev.* 57, 386–420.
- Single, S., Haag, J., and Borst, A. (1997). Dendritic computation of direction selectivity and gain control in visual interneurons. *J. Neurosci.* 17, 6023–6030.
- Struhl, G., and Basler, K. (1993). Organizing activity of wingless protein in *Drosophila*. *Cell* 72, 527–540.
- Sweeney, S.T., Broadie, K., Keane, J., Niemann, H., and O'Kane, C.J. (1995). Targeted expression of tetanus toxin light chain in *Drosophila* specifically eliminates synaptic transmission and causes behavioral defects. *Neuron* 14, 341–351.
- Takemura, S.Y., Karuppudurai, T., Ting, C.Y., Lu, Z., Lee, C.H., and Meinertzhagen, I.A. (2011). Cholinergic circuits integrate neighboring visual signals in a *Drosophila* motion detection pathway. *Curr. Biol.* 21, 2077–2084.
- Takemura, S.Y., Bharioke, A., Lu, Z., Nern, A., Vitaladevuni, S., Rivlin, P.K., Katz, W.T., Olbris, D.J., Plaza, S.M., Winston, P., et al. (2013). A visual motion detection circuit suggested by *Drosophila* connectomics. *Nature* 500, 175–181.
- Tuthill, J.C., Nern, A., Holtz, S.L., Rubin, G.M., and Reiser, M.B. (2013). Contributions of the 12 neuron classes in the fly lamina to motion vision. *Neuron* 79, 128–140.
- van Santen, J.P., and Sperling, G. (1985). Elaborated Reichardt detectors. *J. Opt. Soc. Am. A* 2, 300–321.
- Wang, X., Vaingankar, V., Soto Sanchez, C., Sommer, F.T., and Hirsch, J.A. (2011). Thalamic interneurons and relay cells use complementary synaptic mechanisms for visual processing. *Nat. Neurosci.* 14, 224–231.
- Wasserman, S.M., Aptekar, J.W., Lu, P., Nguyen, J., Wang, A.L., Keles, M.F., Grygoruk, A., Krantz, D.E., Larsen, C., and Frye, M.A. (2015). Olfactory neuro-modulation of motion vision circuitry in *Drosophila*. *Curr. Biol.* 25, 467–472.
- Wertz, A., Borst, A., and Haag, J. (2008). Nonlinear integration of binocular optic flow by DNOVS2, a descending neuron of the fly. *J. Neurosci.* 28, 3131–3140.
- Wylie, D.R., Bischof, W.F., and Frost, B.J. (1998). Common reference frame for neural coding of translational and rotational optic flow. *Nature* 392, 278–282.

# Supplemental Figures

Cell



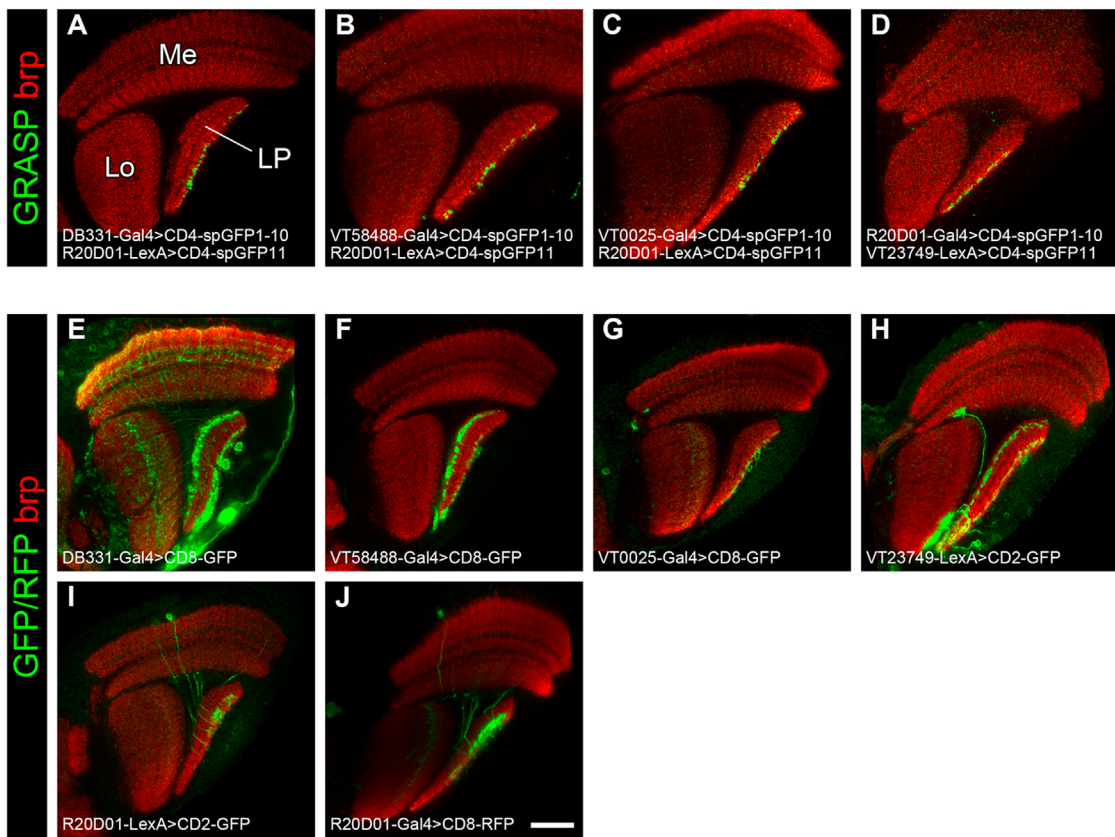


**Figure S2. Membrane Contact between LPi3-4 and VS Cells Labeled by GRASP, Related to Figure 2**

(A–D) GRASP signal is detected in lobula plate (LP) layer 4 using four different LPi3-4/VS cell driver line combinations (Lo, lobula; Me, medulla). (D) is the same confocal image as shown in Figure 2D.

(E–J) Expression patterns of the individual Gal4 and LexA lines used for GRASP experiments.

Scale bar 20  $\mu$ m. Genotypes: (A) DB331-Gal4/+ ; lexAop-CD4-spGFP11, UAS-CD4-spGFP1-10/R20D01-LexA ; +, (B) w<sup>-</sup> ; lexAop-CD4-spGFP11, UAS-CD4-spGFP1-10/R20D01-LexA ; VT58488-Gal4/+, (C) w<sup>-</sup> ; lexAop-CD4-spGFP11, UAS-CD4-spGFP1-10/R20D01-LexA ; VT0025-Gal4/+, (D) w<sup>-</sup> ; lexAop-CD4-spGFP11, UAS-CD4-spGFP1-10/VT23749-LexA ; R20D01-Gal4/+, (E) DB331-Gal4 ; UAS-mCD8-GFP/+ ; +, (F) w<sup>-</sup> ; UAS-mCD8-GFP/+ ; VT58488-Gal4/+, (G) w<sup>-</sup> ; UAS-mCD8-GFP/+ ; VT0025-Gal4/+, (H) w<sup>-</sup> ; VT23749-LexA/+ ; lexAop-CD2-GFP/+ ; R20D01-LexA/+ ; lexAop-CD2-GFP/+ ; (I) w<sup>-</sup> ; R20D01-Gal4/+ ; lexAop-CD2-GFP/+ ; (J) w<sup>-</sup> ; UAS-mCD8-RFP/+ ; R20D01-Gal4/+.

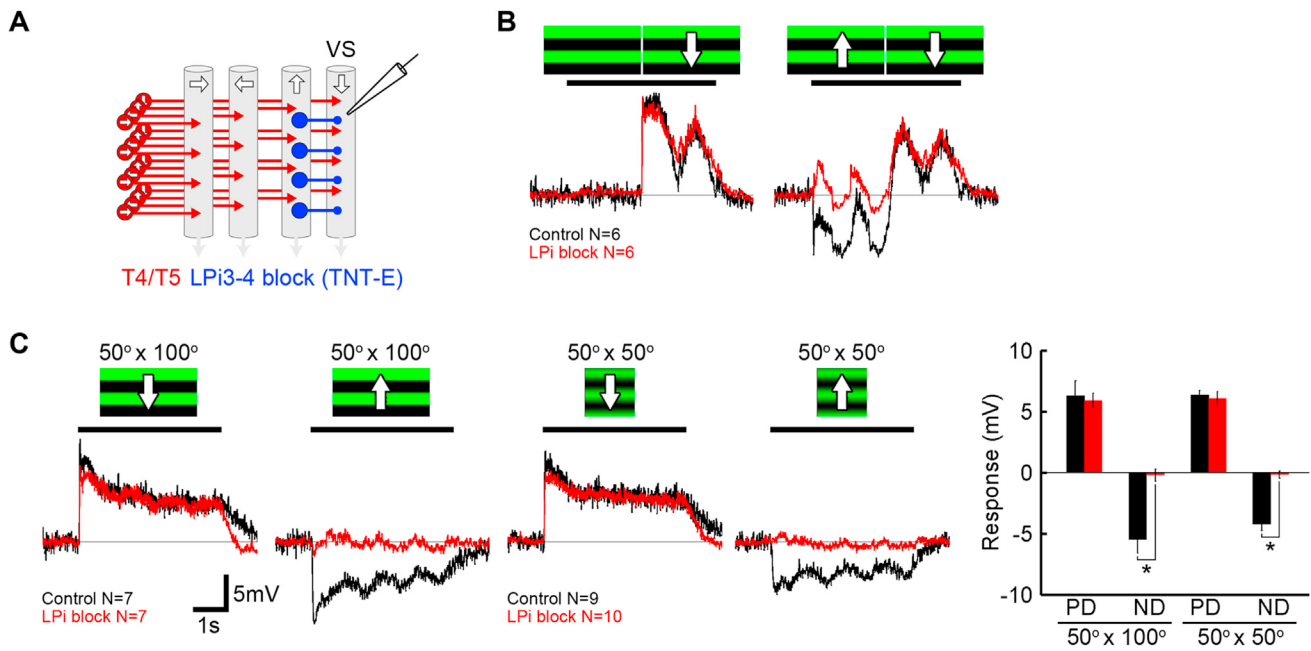


**Figure S3. VS Cell Preferred Direction Responses to Moving Gratings Are Not Affected by the Absence of Null Direction Inhibition, Related to Figure 5**

(A) Schematic to illustrate the experimental approach to probe LPi3-4 cell function by whole cell voltage recordings from VS cells. LPi3-4 output is silenced by TNT-E expression (genotypes as in Figure 5 and 6)

(B) Stimulation with a still grating followed by 2 s downward motion and stimulation with 2 s upward followed by 2 s downward grating motion, moving gratings presented at 1 Hz temporal frequency. For both stimulus conditions, preferred direction excitation is indistinguishable between the control and LPi3-4 block condition, showing that preceding inhibitory stimulus history does not affect the gain of the depolarizing output of tangential cells on a timescale of several seconds.

(C) Stimulation with moving gratings of two sizes: 50° x 100° (square-wave grating) and 50° x 50° (sine-wave grating, data taken from Figure 4B). Gratings were presented at 1 Hz temporal frequency. While null direction responses are selectively abolished in LPi3-4, preferred direction depolarization is identical in both experimental conditions, irrespective of the stimulus window size.

Significant differences were established using a two-tailed Wilcoxon rank-sum test with \* indicating  $p < 0.001$ . Data are represented as mean  $\pm$  SEM.

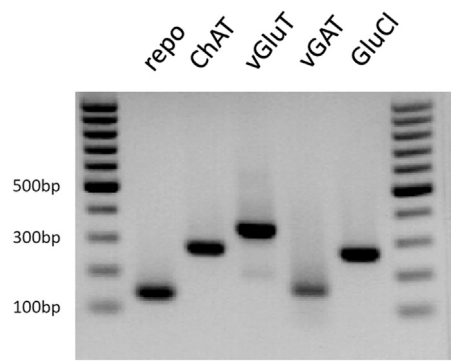


**Figure S4. PCR Amplification of Transcripts Isolated from Whole Heads, Related to Experimental Procedures**

Functionality of gene-specific primers used to detect transcript expression in individual neurons was tested on RNA isolated from heads of Canton S flies. The PCR products detected in the gel match their expected sizes (see [Table S1, Supplemental Experimental Procedures](#)).

**Cell**

**Supplemental Information**

## **Neural Circuit to Integrate**

### **Opposing Motions in the Visual Field**

**Alex S. Mauss, Katarina Pankova, Alexander Arenz, Aljoscha Nern, Gerald M. Rubin,  
and Alexander Borst**

## SUPPLEMENTAL EXPERIMENTAL PROCEDURES

**Flies.** Flies were raised at 25°C and 60% humidity on standard cornmeal agar medium at a 12 h light/dark cycle. The following fly strains were used: *Canton-S wildtype*, *R20D01-Gal4<sup>attP2</sup>* (LPi3-4), *R38G02-Gal4<sup>attP2</sup>* (LPi4-3), *R42F06-Gal4<sup>attP2</sup>* (T4/T5), *R20D01-LexA<sup>attP40</sup>* (LPi3-4), *DB331-Gal4* on X (courtesy of R. Stocker) (Joesch et al., 2008), *VT58488-Gal4<sup>attP2</sup>*, *VT0025-Gal4<sup>attP2</sup>*, *VT23749-LexA<sup>attP40</sup>*, recombined *lexAop-CD4-spGFP11*, *UAS-CD4-spGFP1-10* on 2<sup>nd</sup> (Gordon and Scott, 2009), *UAS-mCD8-GFP* on 2<sup>nd</sup> (all VT, GRASP and CD8-GFP lines courtesy of Barry Dickson), *UAS-synaptotagmin-HA* on 2<sup>nd</sup> (*UAS-syt-HA*, courtesy of Andreas Prokop) (Löhr et al., 2002; Robinson et al., 2002), multicolor flip-out line MCFO-7 (Nern et al., 2015), *UAS-Channelrhodopsin2-H134R-mCherry* on 2<sup>nd</sup> (*UAS-ChR2-H134R*, courtesy of Stefan Pulver) (Mattis et al., 2012; Nagel et al., 2005; Pulver et al., 2009), *norpA<sup>7</sup>* on X (dysfunctional phototransduction mutant EE5) (Hotta and Benzer, 1970), *UAS-stinger-GFP* on 2<sup>nd</sup>, *UAS-GCaMP5G<sup>attP40</sup>* (Akerboom et al., 2012), *UAS-TNT-E* on 2<sup>nd</sup> (Sweeney et al., 1995). If not otherwise indicated, flies were obtained from the Bloomington stock center.

### Genotypes for experiments

#### Figure 1

- (A) *w<sup>-</sup>*; *UAS-synaptotagmin-HA*, *UAS-mCD8-GFP/+*; *R20D01-Gal4/+*  
(B) *w<sup>-</sup>*; *UAS-synaptotagmin-HA*, *UAS-mCD8-GFP/+*; *R38G02-Gal4/+*  
(C–E) *R57C10-Flp2::PEST<sup>attP18</sup>*; +; *pJFRC201-10XUAS-FRT>STOP>FRT-myr::smGFP-HA<sup>VK0005</sup>*, *pJFRC240-10XUAS-FRT>STOP>FRT-myr::smGFP-V5-THS-10XUAS-FRT>STOP>FRT-myr::smGFP-FLAG<sup>su(Hw)attP1</sup>*, *pJFRC210-10XUAS-FRT>STOP>FRT-myr::smGFP-OLLAS<sup>attP2</sup>*/*R20D01-Gal4*  
(F–H) *R57C10-Flp2::PEST<sup>attP18</sup>*; +; *pJFRC201-10XUAS-FRT>STOP>FRT-myr::smGFP-HA<sup>VK0005</sup>*, *pJFRC240-10XUAS-FRT>STOP>FRT-myr::smGFP-V5-THS-10XUAS-FRT>STOP>FRT-myr::smGFP-FLAG<sup>su(Hw)attP1</sup>*, *pJFRC210-10XUAS-FRT>STOP>FRT-myr::smGFP-OLLAS<sup>attP2</sup>*/*R38G02-Gal4*  
(J) *pBPhsFip2::PEST<sup>attP3</sup>*/+; *OL-KD (29C07-KDGeneswitch-4)<sup>attP40</sup>*/+; *R57C10-GAL4<sup>attP2</sup>*, *tubP-KDRT>GAL80-6-KDRT><sup>VK00027</sup>/pJFRC201-10XUAS-FRT>STOP>FRT-myr::smGFP-HA<sup>VK0005</sup>*, *pJFRC240-10XUAS-FRT>STOP>FRT-myr::smGFP-V5-THS-10XUAS-FRT>STOP>FRT-myr::smGFP-FLAG<sup>su(Hw)attP1</sup>*

#### Figure 2

- (A) *w<sup>-</sup>*; *UAS-stinger-GFP/+*; *R20D01-Gal4/+*  
(B) *w<sup>-</sup>*; *UAS-stinger-GFP/+*; *R38G02-Gal4/+*  
(C, left) *w<sup>-</sup>*; *UAS-mCD8-GFP/+*; *R20D01-Gal4/+*  
(C, right) *DB331-Gal4*; *UASmCD8-GFP/+*  
(D) *w<sup>-</sup>*; *lexAop-CD4-spGFP11*, *UAS-CD4-spGFP1-10/VT23749-LexA*; *R20D01-Gal4/+*  
(E, red trace) *norpA<sup>7</sup>*; *UAS-ChR2-H134R*; *R42F06-Gal4*  
(E–H) *norpA<sup>7</sup>*; *UAS-ChR2-H134R*; *R20D01-Gal4*

#### Figure 3

- w<sup>-</sup>*; *UAS-GCaMP5G*; *R20D01-Gal4*  
*w<sup>-</sup>*; *UAS-GCaMP5G*; *R38G02-Gal4*

**Figure 4 to 6**

$w^+ ; + ; R20D01-Gal4$

$w^+ ; UAS-TNT-E ; +$

$w^+ ; UAS-TNT-E ; R20D01-Gal4$

**Immunostaining.** Brains were dissected in PBS and fixed in 4% PFA with 0.1% TritonX for 25 min at room temperature with the exception of anti-vGlut and anti-GAD1 stainings for which brains were fixed in Bouin's fixative (Gregory, 1980) for 5 min at room temperature. Brains were subsequently washed 3-4 times in 0.5% PBT. The primary antibodies used were mouse anti-bruchpilot (nc82, Developmental Studies Hybridoma Bank, 1:200), rabbit anti-GFP (Torrey Pines Biolabs, 1:500), rat anti-HA (Roche, 1:200), chicken anti-GFP (Rockland, 1:500), mouse anti-ChAT (courtesy of P. Salvaterra, 1:200) (Takagawa and Salvaterra, 1996), rabbit anti-vGlut (courtesy of A. DiAntonio, 1:200) (Daniels et al., 2004), rabbit anti-GAD1 (courtesy of F.R. Jackson, 1:200) (Featherstone et al., 2000) and rabbit anti-Tetanus Toxin (Statens Serum Institut, 1:5000). The secondary antibodies all used at 1:500 were goat anti-chicken Alexa Fluor 488, goat anti-rabbit Alexa Fluor 488, goat anti-rabbit Alexa Fluor 568, goat anti-mouse Alexa Fluor 568, goat anti-rat Alexa Fluor 568 (Life Technologies) and goat anti-mouse ATTO 647N (Rockland). 2% normal goat serum was added to all primary and secondary antibody solutions. Brains were mounted (IMM; ibidi) and optically sectioned with a Leica TCS SP5 confocal microscope. Brains expressing GRASP components were fixed, stained against the neuropile marker bruchpilot and mounted as described above. Afterwards, native GRASP fluorescence was visualized.

**Multicolor stochastic labeling.** "Multicolor FlpOut" (MCFO) labeling was carried out as described (Nern et al., 2015). Briefly, low level FLP recombinase expression was used to excise FRT-flanked transcriptional terminators from UAS reporter constructs carrying HA, V5 and FLAG epitope tags, respectively. Epitope tags were visualized by indirect immunofluorescence and images acquired on a Zeiss LSM 710 confocal microscope with a 63x 1.4 NA objective. Images were processed using Janelia Workstation and NeuronAnnotator software (Janelia Fly Light Scientific Computing Team, unpublished). The latter is a modified version of V3aaD (Peng et al., 2010). The images shown are reoriented substack projections generated using NeuronAnnotator and exported as TIFF-format screen shots. Manual segmentation of neurons from MCFO samples was carried out using Fluorender (<http://www.sci.utah.edu/software/fluorender.html>). The VS cell shown in Figures 1J and 1J' was labeled with a method that combines MCFO with a second recombinase system to obtain sparse labeling of optic lobe neurons from a "pan-neuronal" GAL4 driver ("Two-recombinase MCFO", for details see Nern et al. 2015).

**Transcript profiling.** The transcript profiling protocol was modified from the method described previously (Takemura et al., 2011). Lobula plate tangential cells were isolated from the line *DB331-Gal4 ; UAS-mCD8-GFP/+*. Flies were dissected and cells were exposed using the same procedure as for the electrophysiology experiments. For the LPi cells isolation, flies with the genotype  $w^- ; UAS-mCD8-GFP/+ ; R20D01-Gal4/+$  were decapitated and their heads were fixed on a plastic holder with wax. Subsequently, retina and lamina were removed and the medulla was digested with 2 mg/ml Protease Type XIV (Sigma). GFP-expressing somata were harvested using custom-pulled capillaries and kept at -80°C. Five cells were collected into the same tube in order to increase the amount of mRNA for detection. cDNA synthesis

reaction was performed using SuperScript III First-Strand Synthesis SuperMix (Life Technologies). Reactions were primed with random hexamers and carried out exactly as directed by the manufacturer's instructions. Synthesized cDNA was amplified by nested PCR on FlexCycler (Analytik Jena) using DreamTaq Green PCR Master Mix (Thermo Scientific) and gene-specific primers (Table S1). The PCR amplification programs for the first and second round of PCR were as described previously (Takemura et al., 2011). In order to distinguish between PCR products amplified from genomic DNA and cDNA, primers were designed such that they amplified gene regions containing an intron. Size of PCR products was analyzed by agarose gel electrophoresis. For every cDNA synthesis, two control gene sequences were PCR amplified: *mouse CD8* transgene was included as a positive control and glial marker *repo* as a negative control. Functionality of primers used was tested on RNA obtained from heads of Canton S flies. Total RNA was isolated using TRIzol Reagent (Life Technologies), purified with RNeasy Mini Kit (Qiagen) and treated with DNase I, Amplification Grade (Life Technologies). cDNA synthesis and PCR amplification were performed as described above and the expected size of PCR products was confirmed by agarose gel electrophoresis (Figure S4).

**Two-photon calcium imaging.** Two-photon imaging was performed on a custom-built microscope as previously described (Maisak et al., 2013). Images were acquired at a frame rate of 1.88 Hz.

**Electrophysiology.** Electrophysiological experiments were performed as previously described (Mauss et al., 2014). For all experiments 1d old female flies kept at 25°C were used. For optogenetic experiments, yeast paste containing 1 mM all-trans-retinal (ATR, R2500; Sigma Aldrich) was fed to freshly eclosed flies. Using a plastic holder and bees wax, flies were attached beneath a recording chamber with the back of their heads inserted into a small cutout in the bottom of the chamber consisting of thin foil. Under external solution, a window was cut into the head capsule on one side using a hypodermic needle to expose the brain. Further dissection and recordings were performed under a Zeiss AxioTech vario microscope. Under polarized light contrast, the glial sheath was digested locally by applying a stream of 0.5 mg/ml Collagenase IV (Gibco) through a cleaning micropipette (~5 μm opening) (Maimon et al., 2010). Whole cell recordings were established with patch electrodes of 5–8 MΩ resistance. Signals were recorded using a BA-1S bridge amplifier (npi Electronics), low-pass filtered at 3 kHz, and digitized at 10 kHz via an analog/digital converter (PCI-DAS6025; Measurement Computing). All physiological data were acquired in Matlab (R2010b; Mathworks) using the data acquisition toolbox. Normal external solution contained the following (in mM): 103 NaCl, 3 KCl, 5 TES, 10 trehalose, 10 glucose, 3 sucrose, 26 NaHCO<sub>3</sub>, 1 NaH<sub>2</sub>PO<sub>4</sub>, 1.5 CaCl<sub>2</sub>, and 4 MgCl<sub>2</sub>, pH 7.3–7.35, ~280 mOsmol/kg. External solution was carboxygenated (95% O<sub>2</sub>/5% CO<sub>2</sub>) and constantly perfused over the preparation at 2 ml/min. Internal solution, adjusted to pH 7.26 with 1N KOH, contained the following: 140 K-aspartate, 10 HEPES, 4 Mg-ATP, 0.5 Na-GTP, 1 EGTA, 1 KCl, and 0.1 Alexa Fluor 488 hydrazide salt (~265 mOsmol/kg).

**Pharmacology.** Picrotoxinin (PTX; Sigma P8390) was dissolved in dimethylsulfoxide at 50 mM and kept as a stock at -20°C. For experiments, PTX was diluted in external solution to 25 μM and washed in (10 min) and out (30 min) at 2 ml/min.

**Optogenetic stimulation.** Optogenetic stimulation was performed as previously described (Mauss et al., 2014). Light pulses were delivered by a Lambda DG-4 Plus wavelength switcher (Sutter) with a 300W

Xenon Arc lamp via the epifluorescence light path of the microscope through a 40x/0.8 NA water-immersion objective (LUMPlan FI; Olympus). Intensities were measured with a power meter (Thorlabs PM100D) under the objective in air and irradiance per mm<sup>2</sup> estimated, as indicated in Figure 2. Light stimuli were triggered via the data acquisition software with voltage steps. A stimulus trial consisted of eight light pulses interleaved by 5 s.

**Visual stimulation.** Custom-built LED arenas were used for visual stimulation in calcium imaging and electrophysiology experiments. The arenas were engineered and modified based upon Reiser and Dickinson (2008), covered approx. 170° and 90° in azimuth and elevation, respectively, and allowed refresh rates of 550 Hz and 16 intensity levels (Maisak et al., 2013). Identical visual stimuli were presented in 3-5 trials in every experiment, usually in a randomized sequence. Patterns were smoothed by sub-maximal intensity steps so that 4 to 10 frames, depending on the pattern, corresponded to progression across one LED, i.e. pixel. For calcium imaging, stimuli were presented over the whole arena. For the direction tuning (Figure 3C and 3D), square-wave gratings with a spatial wavelength of 24° were shown running at 24°/s (corresponding to a temporal frequency of 1 Hz) in 12 directions separated by angles of 30°. Subsequently shown directions differed by 150° to avoid stimulating neighboring directions in direct succession. For the velocity tuning (Figure 3E and 3F), square-wave gratings with a spatial wavelength of 24° running in the preferred direction were presented at temporal frequencies from 0.05 to 10 Hz. Vertically running ON and OFF edges were presented at a velocity of 30°/s (Figure 3G and 3H). To probe visual VS cell responses in control and LPi block experiments, visual stimuli (except edges and expanding flow fields) were presented fronto-dorsally on the ipsilateral side, to account for GAL4 expression in the LPi3-4 driver line predominantly in cells covering the dorsal visual field. Grating stimuli had the following parameters. Figure 4B: sine-wave grating, 20° spatial wavelength, 1 Hz temporal frequency, 50° x 50° rectangular window; Figure 5A: square-wave grating, 24° spatial wavelength, 1 Hz temporal frequency, 50° diameter round window; Figure 5B: square-wave grating, 24° spatial wavelength, 1 Hz temporal frequency, 50° elevation x 100° azimuth rectangular window; and Figure 5C to E: sine-wave grating, 24° spatial wavelength, dynamic motion, 50° x 50° rectangular window. Horizontal edges (Figure 4C) subtended the full arena and moved vertically at a velocity of 22.5°/s. Four different random motion noise stimuli (Figure 6A) were tested each generated with the same parameters. Each consisted of 100 small squares (4x4 pixels, bright on dark) independently moving in x and y with random trajectories according to a Gaussian velocity distribution ( $\mu = 0^\circ/\text{s}$ ,  $\sigma = 20^\circ/\text{s}$ ). To simulate forward translation (Figure 6B), four random expanding flow fields were generated with the same parameters: 24 objects/s (1 cm half-size, bright on dark) approaching the observer at 10 cm/s and passing at a lateral distance of 10 cm. The angular displacement from the focus of expansion (~34° azimuth, ~0° elevation) can be described by  $\tan^{-1}(d/vt)$  and the angular increase in size of each object by  $2 \cdot \tan^{-1}(l/V(d^2+vt^2))$ , with d denoting lateral distance, l the object half-size, V the approach velocity and t the time to passing. The looming square (Figure 6C) simulated a dark object of 5 cm on a collision course approaching at 10 cm/s. The time-varying angular size  $\theta(t)$  can be described by  $2 \cdot \tan^{-1}(l/vt)$ , with l denoting the object half-size, V the approach velocity and t the time to collision. All patterns except for Figure 5B were shown at full arena contrast.

**Physiological data analysis.** Data from LPi calcium imaging and VS cell recording experiments were evaluated using custom-written analysis scripts in Matlab. *Two-photon calcium imaging:* Time series of relative fluorescence changes ( $\Delta F/F$ ) were calculated from the raw image series. Regions of interest (ROIs) were selected by hand with a diameter of about 1-2  $\mu\text{m}$ , encompassing single putative presynaptic boutons. For every ROI, calcium signals were averaged over 3-5 stimulus repetitions. Visual responses were calculated as the peak amplitude of the average calcium signal during presentation of the respective stimulus subtracted by the preceding baseline calculated from the average of the 2 frames before stimulus presentation. These ROI responses were normalized to the maximum response of this ROI, averaged across ROIs within flies, and then averaged across flies. Only for edge selectivity, single ROIs were considered separately, and their selectivity for ON or OFF edges was quantified using a contrast selectivity index, calculated as  $\text{CSI} = (R_{\text{ON}} - R_{\text{OFF}})/(R_{\text{ON}} + R_{\text{OFF}})$ , with  $R_{\text{ON}}$  an  $R_{\text{OFF}}$  being the baseline subtracted responses to ON and OFF edges, respectively. *Electrophysiology:* To evaluate VS cell responses to optogenetic LPi3-4 stimulation (recorded cells identified anatomically by dye-labeling), eight trials for each cell and condition were averaged and taken for analysis. Those were then averaged across cells and plotted with shaded area as SEM (Figures 2E–2G), or baseline-subtracted minima taken for quantification (Figure 2H). To probe visual tangential cell responses (Figures 4 to 6), cells were selected for robust downward motion responses and after the recording session their VS cell identity could be confirmed by anatomy in most cases. Neurons with lateral receptive fields (~90° azimuth) were discarded right away and three out of eight UAS control flies with both weak preferred and null direction responses were not included in the analysis. Resting membrane potentials of included VS cells (corrected for the experimentally measured liquid junction potential of 11.5 mV) in Gal4 control, UAS control and LPi block flies amounted to  $-51 \text{ mV} \pm 0.4$ ,  $-50 \text{ mV} \pm 0.5$ , and  $-50 \text{ mV} \pm 0.3$  SEM, respectively. Measurements associated with Figure 4, Figures 5A and 5B and Figure S3 were down-sampled to 1 kHz and those associated with Figure 5C and Figure 6 to 0.1 kHz. Responses to four stimuli repetitions were averaged for each cell. In the case of ‘motion noise’ and ‘expanding flow field’ patterns, responses to four trials and four independent patterns (randomly generated with same parameters) were averaged. For quantification, except for edges and looming squares, the membrane potential during 4 s motion was measured and a 1 s baseline prior to motion onset subtracted. To quantify responses to full field edges, a 2 s time window within 4 s stimulation was chosen, in which the edges progressed through the upper half of the arena projecting to the dorsal visual field of the lobula plate, which contains the LPi3-4 cells targeted by the *R20D01-Gal4* driver line (Figure 4A). To quantify responses to the looming stimulus, an arbitrary 2 s response time window was chosen (indicated in Figure 6F). Plotted quantified values in all figures correspond to the mean  $\pm$  SEM. Significant differences were established using a two-tailed Wilcoxon rank-sum test in Matlab.

**Modeling.** Stimuli were calculated at 1° spatial and 10 ms temporal resolution. Every stimulus frame was convolved with a radial Gaussian function of 5° half-width and down-sampled to an array of 40x40 photoreceptors, corresponding to an angular separation of 5° between neighboring receptors. Signals of lamina cells L1 and L2 were calculated by a high-pass filter (time constant 250 ms) plus 10% of the input (Eichner et al., 2011). L1 and L2 signals were processed separately in ON (L1) and OFF (L2) pathways (Joesch et al., 2010): The ON (L1) signal was obtained by half-wave rectifying the signal at a threshold of 0, the OFF (L2) signal was inverted and have-wave rectified at a threshold of 0.05. These signals were

then low- and high-pass filtered within each pathway with time constants of 100 and 300 ms, respectively. To obtain the responses of the 4 groups of T4 and T5 cells (one for each direction), low- and high-pass filtered signals from neighboring columns were multiplied accordingly (e.g. T4a = low-pass left \* high-pass right, T4b = low-pass right \* high-pass left, etc.). T4 and T5 signals were then half-wave rectified with a threshold of 0.005. The signal of VS cells in control flies was calculated as the spatial sum of all 40x40 T4d and T5d cells (i.e. downward tuned) minus the sum of all T4c and T5c cells (i.e. upward tuned). To simulate the condition of LPi block, the VS cell signal was calculated without subtraction of T4c and T5c cells.

**Table S1. Primer pairs used for the PCR amplification of gene-specific sequences, Related to Experimental Procedures**

Gene	First-round primers (5' - 3')	Nested primers (5' - 3')	Expected nested PCR product size	
			Template: DNA	Template: cDNA
mouse CD8	-	F: AAGGTGGACCTGGTATGTGAAGTG R: ACCGAGTTGCTGATGACTGAG	266 bp	266 bp
Repo (CG31240)	F: GAAGCAGCAGCAAGAAGAAGG R: CACGGGATTCGCTCAGATTCA	F: GGCATCAAGAAGAAGAACG R: GATTGCGCTCAGATTCAAGCTTG	552 bp	137 bp
ChAT (CG12345)	F: ACCGGGAAATGCTTCAGGAG R: GTCCACACTTGGAGGCTT	F: GCAATCAACGCAATCTGGAGC R: GGAACAGGAGTGCTCATAGCA	336 bp	272 bp
vGlut (CG9887)	F: TCCCGGCCAACAAAGATATT R: AACTTGTGCTTGAGGAACG	F: TGCATCTCTCGTGCCATT R: GTATGCTGATGGCCGGATGTT	807 bp	339 bp
vGAT (CG8394)	F: GCCCGTATAGCAGCAGATGT R: CAGCAAACGGACGGCTTAG	F: GCGATACGATGAACATGCC R: CAGCAAACGGACGGCTTAG	223 bp	151 bp
GluCl $\alpha$ (CG7535)	F: GACGGATGAACGCCCTCAAGT R: TTCTCCAGTGTGAAGCGAGG	F: TCGAACGAGAAGGGAGGGACA R: GTGTGAAGCGAGGTAGGTGT	533 bp	265 bp

## SUPPLEMENTAL REFERENCES

- Akerboom, J., Chen, T.-W., Wardill, T., Tian, L., Marvin, J., Mutlu, S., Calderón, N., Esposti, F., Borghuis, B., Sun, X., et al. (2012). Optimization of a GCaMP calcium indicator for neural activity imaging. *J Neurosci* 32, 13819-13840.
- Daniels, R., Collins, C., Gelfand, M., Dant, J., Brooks, E., Krantz, D., and DiAntonio, A. (2004). Increased expression of the *Drosophila* vesicular glutamate transporter leads to excess glutamate release and a compensatory decrease in quantal content. *J Neurosci* 24, 10466-10474.
- Eichner, H., Joesch, M., Schnell, B., Reiff, D., and Borst, A. (2011). Internal structure of the fly elementary motion detector. *Neuron* 70, 1155-1164.
- Featherstone, D.E., Rushton, E.M., Hilderbrand-Chae, M., Phillips, A.M., Jackson, F.R., and Broadie, K. (2000). Presynaptic glutamic acid decarboxylase is required for induction of the postsynaptic receptor field at a glutamatergic synapse. *Neuron* 27, 71-84.
- Gordon, M.D., and Scott, K. (2009). Motor control in a *Drosophila* taste circuit. *Neuron* 61, 373-384.
- Gregory, G.E. (1980). The bodian protargol technique. In *Neuroanatomical Techniques: Insect Nervous System*, N.J. Strausfeld, and T.A. Miller, eds. (Springer Verlag New York), pp. 75-95.
- Hotta, Y., and Benzer, S. (1970). Genetic dissection of the *Drosophila* nervous system by means of mosaics. *Proc Natl Acad Sci U S A* 67, 1156-1163.
- Joesch, M., Plett, J., Borst, A., and Reiff, D. (2008). Response properties of motion-sensitive visual interneurons in the lobula plate of *Drosophila melanogaster*. *Curr Biol* 18, 368-374.
- Joesch, M., Schnell, B., Raghu, S., Reiff, D., and Borst, A. (2010). ON and OFF pathways in *Drosophila* motion vision. *Nature* 468, 300-304.
- Löhr, R., Godenschwege, T., Buchner, E., and Prokop, A. (2002). Compartmentalization of central neurons in *Drosophila*: a new strategy of mosaic analysis reveals localization of presynaptic sites to specific segments of neurites. *J Neurosci* 22, 10357-10367.
- Maimon, G., Straw, A., and Dickinson, M. (2010). Active flight increases the gain of visual motion processing in *Drosophila*. *Nat Neurosci* 13, 393-399.
- Maisak, M.S., Haag, J., Ammer, G., Serbe, E., Meier, M., Leonhardt, A., Schilling, T., Bahl, A., Rubin, G.M., Nern, A., et al. (2013). A directional tuning map of *Drosophila* elementary motion detectors. *Nature* 500, 212-216.
- Mattis, J., Tye, K., Ferenczi, E., Ramakrishnan, C., O'Shea, D., Prakash, R., Gunaydin, L., Hyun, M., Fenno, L., Grdinaru, V., et al. (2012). Principles for applying optogenetic tools derived from direct comparative analysis of microbial opsins. *Nature Methods* 9, 159-172.
- Mauss, A.S., Meier, M., Serbe, E., and Borst, A. (2014). Optogenetic and pharmacologic dissection of feedforward inhibition in *Drosophila* motion vision. *J Neurosci* 34, 2254-2263.
- Nagel, G., Brauner, M., Liewald, J., Adeishvili, N., Bamberg, E., and Gottschalk, A. (2005). Light activation of channelrhodopsin-2 in excitable cells of *Caenorhabditis elegans* triggers rapid behavioral responses. *Curr Biol* 15, 2279-2284.
- Nern, A., Pfeiffer, B.D., and Rubin, G.M. (2015). Optimized tools for multicolor stochastic labeling reveal diverse stereotyped cell arrangements in the fly visual system. *Proc Natl Acad Sci U S A* 112, E2967-2976.

- Peng, H., Ruan, Z., Long, F., Simpson, J.H., and Myers, E.W. (2010). V3D enables real-time 3D visualization and quantitative analysis of large-scale biological image data sets. *Nat Biotechnol* 28, 348-353.
- Pulver, S., Pashkovski, S., Hornstein, N., Garrity, P., and Griffith, L. (2009). Temporal dynamics of neuronal activation by Channelrhodopsin-2 and TRPA1 determine behavioral output in *Drosophila* larvae. *J Neurophysiol* 101, 3075-3088.
- Reiser, M., and Dickinson, M. (2008). A modular display system for insect behavioral neuroscience. *J Neurosci Methods* 167, 127-139.
- Robinson, I., Ranjan, R., and Schwarz, T. (2002). Synaptotagmins I and IV promote transmitter release independently of Ca(2+) binding in the C(2)A domain. *Nature* 418, 336-340.
- Struhl, G., and Basler, K. (1993). Organizing activity of wingless protein in *Drosophila*. *Cell* 72, 527-540.
- Sweeney, S., Broadie, K., Keane, J., Niemann, H., and O'Kane, C. (1995). Targeted expression of tetanus toxin light chain in *Drosophila* specifically eliminates synaptic transmission and causes behavioral defects. *Neuron* 14, 341-351.
- Takagawa, K., and Salvaterra, P. (1996). Analysis of choline acetyltransferase protein in temperature sensitive mutant flies using newly generated monoclonal antibody. *Neurosci Res* 24, 237-243.
- Takemura, S.Y., Karuppusudurai, T., Ting, C.Y., Lu, Z., Lee, C.H., and Meinertzhagen, I. (2011). Cholinergic circuits integrate neighboring visual signals in a *Drosophila* motion detection pathway. *Curr Biol* 21, 2077-2084.